Journal of Foraminiferal Research, v. 29, no. 4, p. 392–417, October 1999

FORAMINIFERAL ASSEMBLAGE AND STABLE ISOTOPIC CHANGE ACROSS THE CENOMANIAN–TURONIAN BOUNDARY IN THE SUBTROPICAL NORTH ATLANTIC

BRIAN T. HUBER[1], R. MARK LECKIE[2], RICHARD D. NORRIS[3], TIMOTHY J. BRALOWER[4], AND EMILY COBABE[2]

ABSTRACT

The Cenomanian/Turonian boundary interval (CTBI) at Site 1050 (30°6′N, 76°14′W) was investigated to characterize climatic and oceanographic changes during the Oceanic Anoxic Event that was associated with it (OAE 2). Because of unusually good foraminiferal preservation for sediments of this age, we have obtained an unaltered oxygen and carbon isotope profile and an accompanying record of planktic and benthic foraminifer abundance changes across the OAE 2 interval. Biostratigraphic, sedimentologic, and chemostratigraphic analyses indicate that more than 0.5 m.y. between the onset and tail end of OAE 2 are missing. This explains why organic-rich sediments are absent from the Site 1050 sequence and why the planktic and benthic carbon isotope shifts are minor (~0.8‰) compared with the most complete OAE 2 sections.

While planktic species diversity shows relatively minor change across the OAE 2 interval, extinction of the rotaliporids and *Globigerinelloides bentonensis*, a shift to *Heterohelix*-dominated assemblages, and increased abundance of helvetoglobotruncanids at the onset of OAE 2 cause a dramatic change in the planktic foraminifer assemblage composition. The rotaliporid extinction occurs at the level where middle bathyal temperatures are estimated to have increased from 15 to 19°C, which is warmer than any other time during the Cretaceous and Cenozoic. This deep water warming may have caused a breakdown in the vertical structure of the water column, and could explain the extinction of deeper dwelling planktic species, including *Rotalipora* and *G. bentonensis*. On the other hand, sea surface temperature estimates based on planktic foraminiferal $\delta^{18}O$ values (corrected for salinity) remain steady throughout the CTBI, varying between 23 to 26°C.

The presence of volcaniclastic sediments within the OAE 2 interval at Site 1050 is consistent with previous suggestions that the CTBI was a time of anonymously high rates of CO_2 flux into the atmosphere and oceans during a major phase of explosive volcanic activity and large igneous province emplacement in the Caribbean and other regions worldwide. Further investigation of the CTBI is needed to establish whether increased pCO_2 can be accepted as the primary forcing mechanism for the middle Cretaceous "supergreenhouse".

INTRODUCTION

The Cenomanian/Turonian boundary interval (CTBI) can be correlated globally in pelagic carbonate facies by a biotic turnover in planktic foraminifers and molluscs, and by a positive carbon isotopic excursion typically near or within dark marls or shales that are enriched in organic carbon (Schlanger and others, 1987). Enhanced preservation of organic matter at this and several other times during the mid-Cretaceous probably resulted from global expansion of the oxygen minimum zone during "Oceanic Anoxic Events" (OAEs; Schlanger and Jenkyns, 1976). The cause of the mid-Cretaceous OAEs has been widely debated, however, as most authors regard their occurrences as the result of the interplay between global warmth, high global eustatic sea level, and increased surface water productivity and/or deep water stagnation (Schlanger and Jenkyns, 1976; Bralower and Thierstein, 1984; Schlanger and others, 1987; Arthur and others, 1987; Thurow and others, 1992a; Bralower and others, 1993; Erbacher and others, 1996).

At the time of the Cenomanian/Turonian boundary OAE, which is also known as OAE 2 (Schlanger and others, 1987) or the Bonarelli Event (Arthur and Premoli Silva, 1982), an increase in seafloor spreading rates caused global sea level to rise to the highest level of the past 250 m.y. (Haq and others, 1987; Sahagian and others, 1996) and the Earth's climate was extremely warm and equable (Barron and Washington, 1985). Arthur and others (1987) postulated that this led to a dramatic increase in the formation of warm, saline bottom water, increased rates of oceanic turnover and upwelling of nutrient-rich deep water masses, and high surface-water productivity. They suggested that the resulting higher flux of organic carbon to the seafloor caused oxygen depletion and loss of burrowing or infaunal biota from seafloor settings where organic-rich sediments accumulated. The positive carbon isotopic shift within OAE 2 is considered by these authors to be the result of removal of ^{12}C from the ocean reservoir and relative enrichment in the oceans of the heavier carbon isotope. Correlation of this carbon isotopic shift has confirmed its global synchroneity, with peak $\delta^{13}C$ values occurring at the base of the planktic foraminiferal *Whiteinella archaeocretacea* Zone in the latest Cenomanian (Scholle and Arthur, 1980; Schlanger and others, 1987). The duration of OAE 2 is estimated to be about 0.5 m.y. (Arthur and others, 1987; Thurow and others, 1992a).

Oxygen depletion and eutrophication of the oceans have been attributed as the cause for a major turnover within numerous biotic groups during OAE 2 in deep sea as well as marginal marine environments (e.g., Caron and Homewood, 1983; Leckie, 1985; Jarvis and others, 1988; Kaiho and Hasegawa, 1994; Elder, 1991; Boulter and others, 1998). Selective extinction of deeper dwelling species of planktic foraminifera (particularly the single-keeled rotaliporids) and radiolarians at the time of the $\delta^{13}C$ excursion

[1] Department of Paleobiology, NHB-121, Smithsonian Institution, Washington, DC 20560.
[2] Department of Geosciences, University of Massachusetts, Amherst, MA 01003.
[3] Woods Hole Oceanographic Institute Woods Hole, MA 02543.
[4] Department of Geological Sciences, CB3315., Mitchell Hall, University of North Carolina, Chapel Hill, NC 27599-3315.

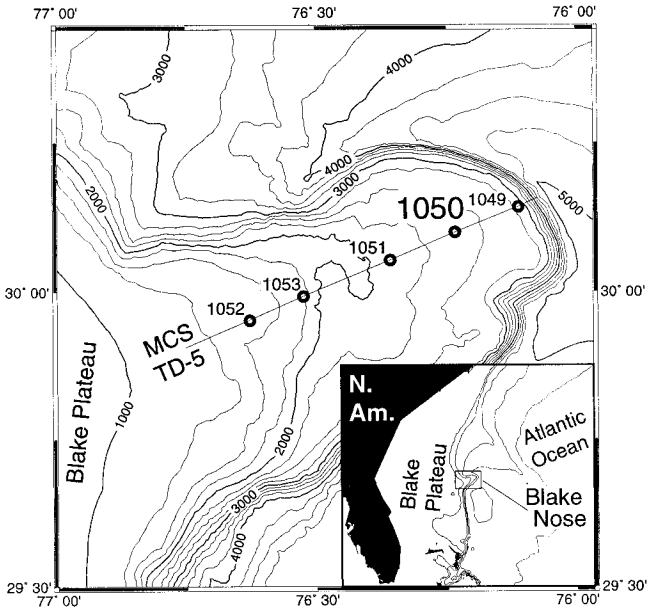

FIGURE 1. Map showing locations of Site 1050 and other sites drilled during the ODP Leg 171B depth transect on Blake Nose.

has been used as evidence for expansion of the oxygen minimum zone (OMZ) into the deep mixed layer of the world oceans (Hart, 1980; Leckie, 1985; Arthur and others, 1987; Thurow and others, 1992b; Erbacher and Thurow, 1997). As the OMZ weakened, new species gradually evolved into the niches that were vacated by the extinct species (Jarvis and others, 1988; Leckie, 1989).

In this paper we present new oxygen and carbon isotope data and planktic foraminifer abundance counts across the CTBI of Ocean Drilling Program (ODP) Hole 1050C, which is located on Blake Nose in the subtropical western North Atlantic (Fig. 1). Only a short interval of OAE 2 is preserved at Site 1050 because of the presence of several diastems and local slumping. Nonetheless, the unusually good preservation of the recovered calcareous microfossils affords a unique opportunity to reconstruct changes in planktic foraminifer population structure and estimate oxygen isotopic paleotemperatures of intermediate and surface waters at this time of major oceanographic change. Possible relationships between the isotopic and biostratigraphic profiles will be explored in light of oceanographic models that have been developed to explain the causes and effects of the Cenomanian/Turonian boundary event.

GEOLOGIC SETTING

Hole 1050C was rotary cored on the deep, seaward end of Blake Nose in 2308 m water depth at 30°6′N, 76°14′W (Fig. 1). Because continental margin subsidence was largely complete by Early Cretaceous time (Benson, Sheridan, and others, 1978) and sea level of the mid-Cretaceous was much higher than at present, it is likely that Blake Nose occupied a similar depth as today during the CTBI. Seismic records reveal the presence of buried reef buildups at the landward end of Blake Nose and fore-reef deposits and pelagic oozes that gently slope and gradually thin eastward to the Blake Escarpment, where the continental margin drops sharply to the abyssal plain. Most of the sedimentary cover on Blake Nose is composed of an 8- to 12-km thick sequence of Jurassic and Lower Cretaceous limestones. This is capped by less than 1 km of Upper Cretaceous and Paleogene chalks and marls (Benson, Sheridan, and others, 1978).

The Leg 171B depth transect on Blake Nose revealed that the Cenomanian sequence expands considerably (~70 m) from the margins to the center of this feature (Norris and others, 1998). Cenomanian strata are completely absent from the section at Site 1049, which was drilled on a small paleo-high near the northeast tip of Blake Nose (Fig. 1). Turonian through lower Campanian sediments were cored only at Site 1050.

LITHOSTRATIGRAPHY

Cretaceous sediments at Site 1050, cored from 404 to 606 meters below seafloor (mbsf), consist of nannofossil claystone and nannofossil chalk and range from upper Albian through upper Maastrichtian. Lithologic description and the general chronostratigraphy are presented in Norris and others (1998). The upper Albian-upper Cenomanian interval is ~100 m thick and was deposited at a sedimentation rate that averages about 10 m/m.y. while the Maastrichtian is ~70 m thick, and was deposited at an average sedimentation rate of about 17 m/m.y. On the other hand, the Turonian through lower Campanian is extremely condensed within a 20 m interval (between 500 and 480 mbsf) of hardgrounds and nannofossil chalk. Slumping occurs at a number of intervals in the Cenomanian-Maastrichtian section. These slumps appear to have been locally derived and have not resulted in discernable stratigraphic repetition.

The sediments considered in this study (509–495 mbsf) span from the core-catcher of Core 1050C-21R, which is assigned to the upper Cenomanian *Rotalipora cushmani* Zone, through the top of Section 1050C-20R-4, which is placed in the middle Turonian portion of the *Helvetoglobotruncana helvetica* Zone. The percentage of carbonate through most of this interval is high, varying between 80 and 90%, but decreases to 14% within a sharply defined, dark red claystone layer at 500.78–500.81 mbsf (Fig. 2). Total organic carbon (TOC) is low for all samples, ranging between 0.01 and 0.03%. One sample that is slightly enriched in TOC relative to the others occurs in a dark marly layer at 508.81 mbsf, but this only amounts to 0.66% TOC.

The most distinctive interval of the 15 m sequence occurs between 55 and 76 cm within section 1050C-21R-1 (500.75–500.96 mbsf). Rounded to flattened clay clasts that are variable in size and up to 2 cm across occur floating in a white- and gray-colored chalk matrix (Figs. 2, 3). The lack of size sorting of the clay clasts and sharply defined basal contacts of the white and gray clast-bearing intervals suggest that these were deposited by two (possibly three) debris flows (Norris and others, 1998, p. 110). The top of the second debris flow also shows a sharp contact, suggesting that this too is a scour surface.

X-ray diffraction, microprobe, and stereomicroscopic study of the clay have revealed that the clasts are entirely composed of magnesium-rich smectite and are devoid of microfossils. The Mg enrichment of the smectite and ob-

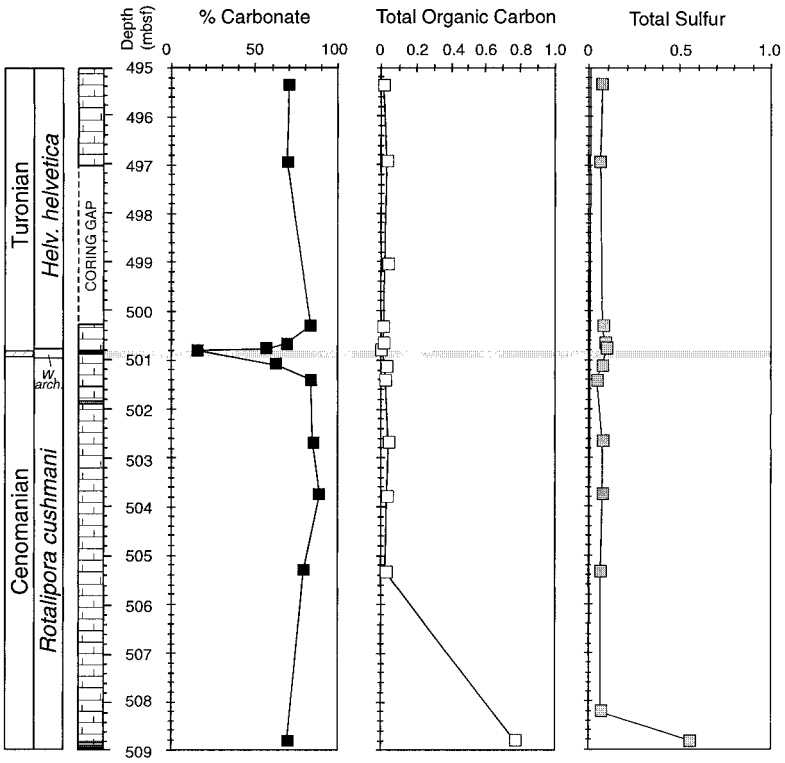

FIGURE 2. Lithostratigraphy of the Cenomanian–Turonian boundary sequence relative to the percent carbonate, total organic carbon, (TOC), and total sulfur content.

servations of crystalline ghosts with the clasts suggest that the smectite was altered from a volcanic ash that was deposited in a marine environment (J. Post, pers. comm., 1999).

VOLCANISM

Widespread volcanism occurred around the northern and western rim of the Gulf of Mexico basin margin during Late Cretaceous time (Byerly, 1991). This intraplate volcanic activity may be related to tectonic stresses along weakened ancient plate boundaries caused by global plate reorganizations and/or isostatic adjustments. In general, the Upper Mesozoic volcanic rocks across this region are alkaline in composition. The closest volcanism to Blake Nose occurred in the southern Mississippi Embayment. The Murfreesboro lamproite diatreme is located just south of the Ouachita Mountains, in Pike County Arkansas. It is composed of diamond-bearing ultrapotassic rocks that have been interpreted as an explosive pipe (Byerly, 1991). The Murfreesboro lamproite has a poorly constrained age of Albian-Cenomanian (106 ± 3, 97 ± 2 Ma). Cretaceous kimberlites are also known from Oklahoma and Kansas. The Monroe uplift, a broad structural platform created during Late Cretaceous time across northeast Louisiana, southeast Arkansas, and west-central Mississippi, consists of widespread volcanic and hypabyssal rocks, much of which occurs today in the subsurface. Lamprophyres are the most common rock type. Only two radiometric ages have been reported from the area: 91 ± 3 Ma and 78 ± 3 Ma, the latter is interpreted as either a cooling age (intrusive) or an apparent age due to alteration (Byerly, 1991). The Monroe uplift volcanoes supplied abundant volcaniclastic material to the adjacent basins during Cenomanian time (Spooner, 1964). The Jackson dome of central Mississippi is a 40 km-wide feature created by volcanic activity during the Cenomanian. These volcanoes formed a complex of islands composed of phonolitic lavas, pyroclastics and minor lamprophyres (Byerly, 1991).

Tephra from volcanoes of the southern Mississippi Embayment may have been the source of smectite-rich clay clasts in the CTBI of Hole 1050C (Fig. 3). The low TOC and sulfur content from the smectite-rich layers are consistent with this interpretation, since these values would be expected to increase if the clay had a detrital origin. Numerous altered tephra layers were found in Upper Cretaceous and Cenozoic strata of the Caribbean Sea during ODP Leg 165 (Sigurdsson, Leckie, Acton and others, 1997). Like the clay clasts of Hole 1050C (see below), the altered Caribbean tephras are homogeneous and non-calcareous (non-fossiliferous).

EUSTASY

Global sea level was on the rise during the time of the Cenomanian–Turonian boundary (Fig. 4). For example, the latest Cenomanian (*Sciponoceras gracile* or correlative *Metoicoceras geslinianum* ammonite Zones) is marked by a major incursion of warm, tropical, normal marine water masses and biota into the Western Interior Sea (WIS) of the U.S. and Canada (e.g., Kauffman, 1977, 1984; Leckie and others, 1998). An abrupt increase in bioturbation from shoreface to basinal facies across the WIS at the base of the *S. gracile* ammonite Zone attests to the wholesale oceanographic changes, including substrate composition and ben-

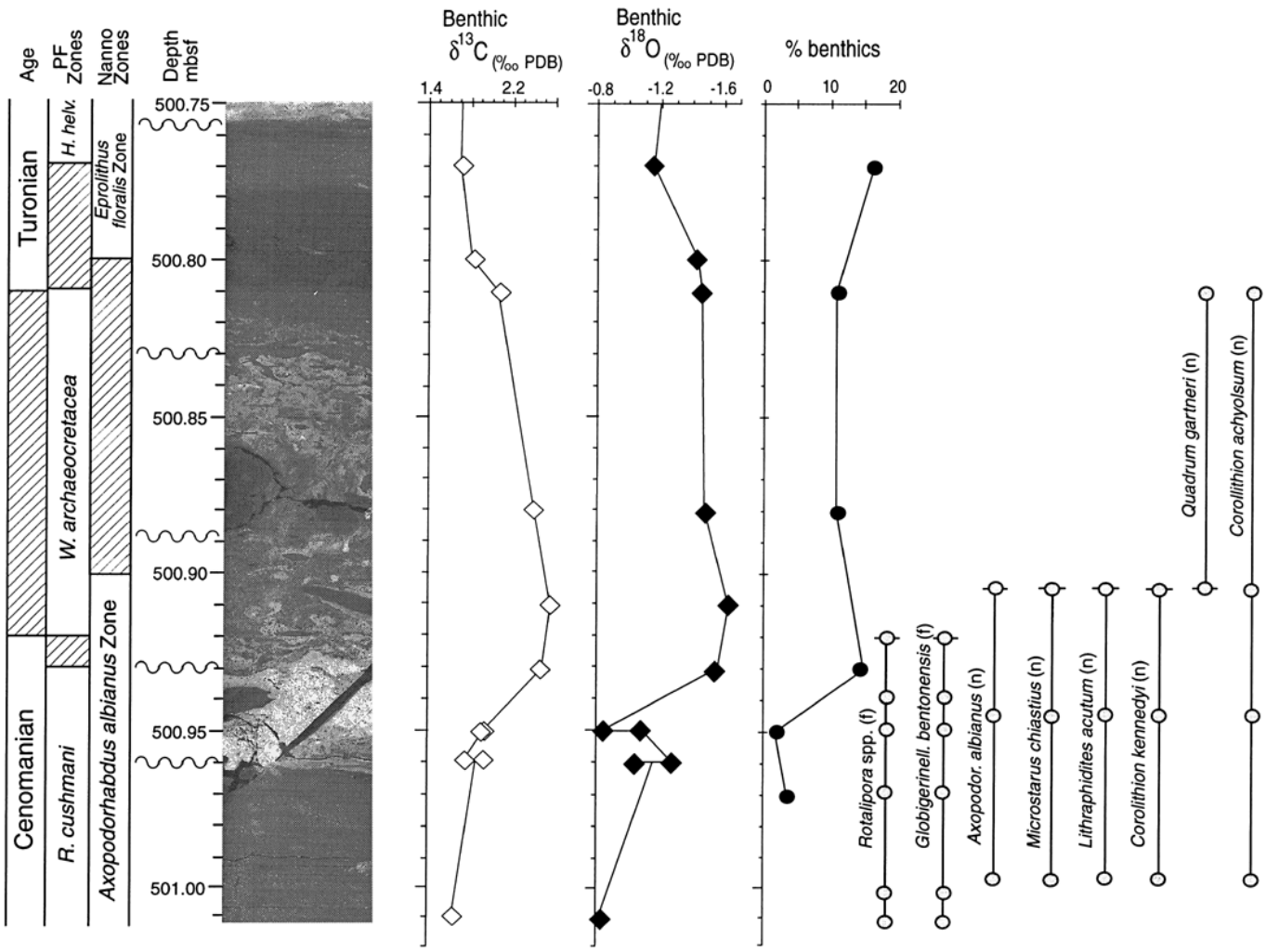

FIGURE 3. Enlarged view of Section 1050C-21R-1, 55–81 cm showing large, irregular-shaped clay clasts floating in a white and gray colored chalky marl. This interval is interpreted as multiple debris flows. Note the significant change in stable isotopic and benthic foraminifer composition across the contact of the two debris flow beds. Lithologic breaks bounding and within the debris flow bed interval and at 500.755 mbsf are identified as diastems (symbolized by wavy lines). The dark interval between 500.78 and 500.81 mbsf is red-colored clay that contains abundant planktic and benthic foraminifera and has the lowest % carbonate of the sequence. Stratigraphic occurrences of planktic foraminifera (f) and calcareous nannofossils (n) are also illustrated. Horizontal lines at range terminations represent species first or last occurrences.

thic oxygenation, associated with this flooding event (Elder and others, 1994). Transgression is recorded at many localities around the world at this time (e.g., Schlanger and others, 1987; Robaszynski and others, 1990, 1993; Thurow and others, 1992; Sahagian and others, 1996). The Plenus Marl Formation of the Anglo-Paris Basin, southeast England and northern France (Jarvis and others, 1988), and the Plenus Bed of the Lower Saxony Basin, Northwest Germany (Hilbrecht and Dahmer, 1994) record a transgressive episode marking the onset of OAE 2. The LO of the planktic foraminifer *Rotalipora cushmani* occurs in the lower part of this widespread unit.

The white marl in Core 1050C-21R-1, 500.93–500.96 mbsf (Fig. 3), is latest Cenomanian in age (see below). This distinctive lithology may correlate with transgression and the deposition of the basal Plenus Marl (Jarvis and others, 1988; Pratt and others, 1993; Hilbrecht and Dahmer, 1994; Paul and others, 1994; Sageman and others, 1997).

METHODS

Five to 10 cc core samples were soaked in a 3% solution of hydrogen peroxide mixed with a small amount of Calgon, warmed on a hotplate, cleaned in an ultrasonic bath, washed with tap water over a 63 μm sieve, and then dried on the sieve over a hotplate at ~50°C. To avoid biasing the populations sieved residues were split into a larger fraction that was picked for stable isotope analysis and a smaller fraction that was used for census counts.

BIOSTRATIGRAPHIC METHODS

Foraminifer sample preservation generally ranged from good (= little evidence of overgrowth, dissolution, or abrasion) to moderate (= calcite overgrowth, dissolution, or abrasion are common but minor).

Morphogroup abundance counts across the CTBI from 495 to 510 mbsf were performed on the >63 μm size frac-

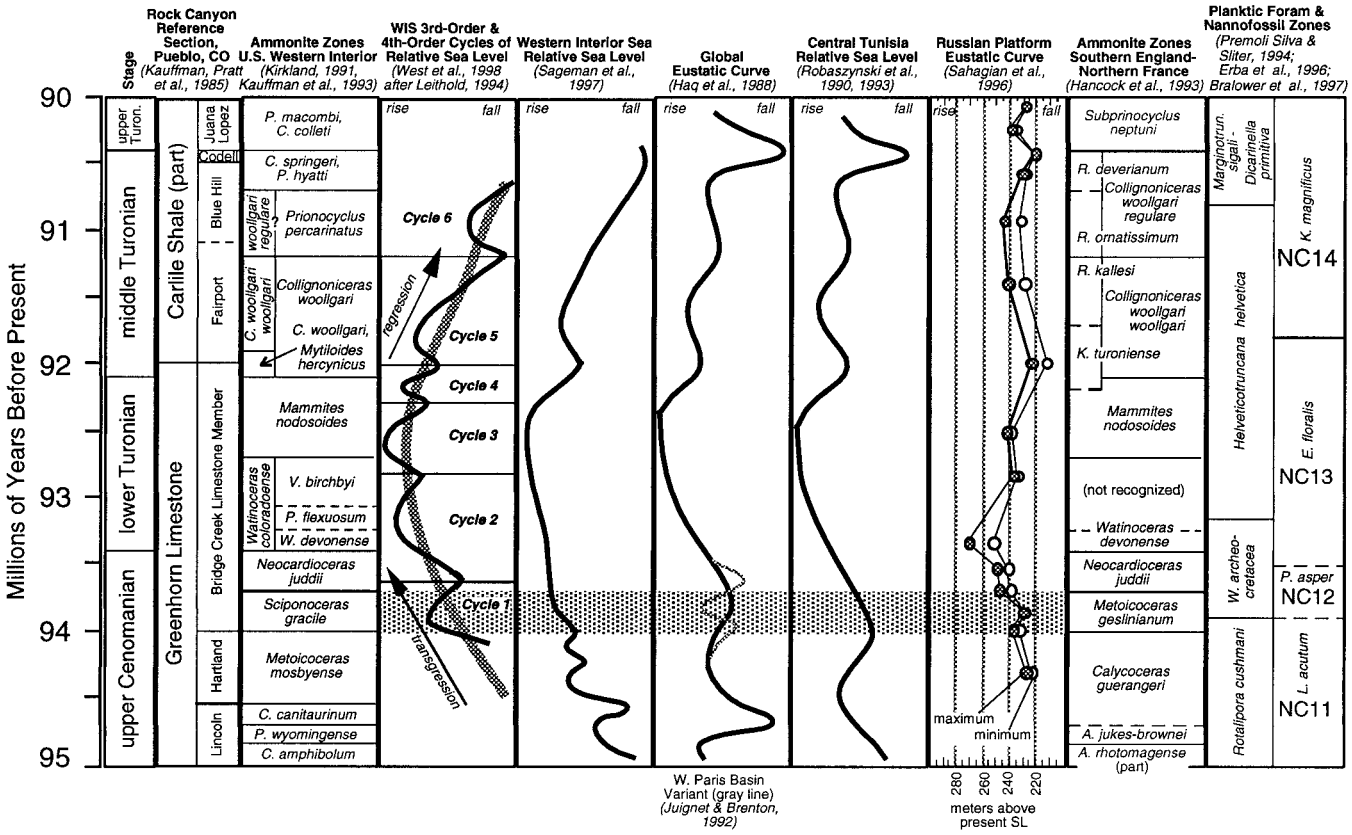

FIGURE 4. Global and regional sea level curves for the upper Cenomanian-Turonian consistently showing peak transgression within the lower *Helvetoglobotruncana helvetica* Zone during the early Turonian. The shaded band across the latest Cenomanian shows the timing of rapid sea level rise and tropical water incursion into the Western Interior Sea (WIS), and the deposition of the transgressive Plenus Marl/Plenus Bed in northwest and north-central Europe.

tion to characterize general trends among the planktic foraminiferal assemblages that would be missed using a larger size fraction and to determine benthic/planktic ratios. Samples were split to a small size using an Otto microsplitter, evenly scattered on a gridded picking tray, and grid transects were counted until >300 specimens were picked. All counted specimens were identified and sorted on labeled microslides. These data are presented in Table 1 and summarized in Figures 5 and 6.

Morphotype categories include the following genera:

Morphotype	Genera
Biserial	*Heterohelix*
Planispiral	*Globigerinelloides*
Trochospiral	*Hedbergella, Whiteinella*
Single-keeled	*Praeglobotruncana, Rotalipora, Helvetoglobotruncana*
Double-keeled	*Dicarinella, Marginotruncana*
Other	*Guembelitria, Schackoina*

The abundance of other sedimentary constituents, such as glauconite, fish bone and teeth, molluscan shell fragments, pyrite, etc. were recorded and are noted in the text.

Species abundance counts were obtained from the >125 μm size fraction only for Section 1050C-21R-1 to carefully document population changes across the OAE 2 interval. The counting method used was the same as described above for the >63 μm fraction. Specimens that were unidentifiable to the species level were categorized using open nomenclature, and specimens unidentifiable at the genus level were included in the "Other" category. These data are presented in Table 2 and Figures 7 and 8.

Relative abundance estimates were determined for samples that were not sufficiently well-preserved for reliable abundance counts. The abundance categories were defined as follows:

Present (P): <0.1%
Rare (R): 0.1–5%
Few (F): 5–10%
Common (C): 10–30%
Abundant (A): >30%
Reworked (r): specimen derived from older sediment

The abundances of the identified taxa were used to estimate species richness, H(S) diversity, and equitability through the section (Fig. 9). Species richness (S) is the total number of species observed in any sample without normalizing for sample size. H(S) diversity was calculated using the Information Function (Shannon, 1948)

$$H(S) = \sum p_i \ln p_i$$

for i = 1 to the number of species observed where p_i, is the proportion of the total sample represented by the ith species. This function characterizes a population, taking into account

TABLE 1. Numerical abundance data for benthic foraminifera and planktic foraminifer morphotypes from the >63 μm size fraction. See text for listing of genera included in each morphotype category.

HOLE 1050C	Top depth	Keeled	Trochospiral	Planispiral	Biserial	Other	Tot. planktics	Tot. benthics
20R-4, 29-32	495.34	3	183	14	65	0	265	66
20R-4, 61.5-62.5	495.67	11	99	11	227	2	350	6
20R-4, 110-111	496.15	5	141	7	275	5	433	13
20R-4, 120-121	496.30	12	171	1	62	1	247	87
20R-5, 7-8	496.62	6	152	2	231	1	392	11
20R-5, 18-19	496.73	11	126	2	300	3	442	6
20R-5, 27-28	496.82	7	96	5	257	4	369	9
20R-5, 37-38	496.92	9	133	3	280	3	428	7
21R-1, 0-1	500.20	16	133	2	152	0	303	6
21R-1, 10-11	500.30	6	106	1	230	1	344	5
21R-1, 20-21	500.40	7	96	3	223	1	330	8
21R-1, 31-34	500.51	8	81	3	237	0	329	5
21R-1, 42-43	500.62	23	99	6	201	2	331	5
21R-1, 47-48	500.67	7	96	2	226	1	332	12
21R-1, 56.5-57.5	500.77	7	154	6	145	3	315	61
21R-1, 61-62	500.81	17	195	8	124	3	347	42
21R-1, 68-69	500.88	20	163	7	112	2	304	37
21R-1, 72-73	500.92	49	159	1	59	4	272	48
21R-1, 75-76	500.95	27	191	32	83	1	334	6
21R-1, 76.5-77.5	500.97	29	209	27	67	2	334	12
21R-1, 81-82	501.01	7	166	23	108	6	310	1
21R-1, 92-93	501.12	2	192	9	127	3	333	11
21R-1, 105-108	501.25	8	224	19	147	7	405	17
21R-1, 120-121	501.40	9	167	9	139	4	328	13
21R-1, 135-136	501.55	5	185	11	105	2	308	20
21R-3, 56-59	503.76	3	323	19	67	1	413	14
21R-6, 54-57	508.24	3	267	19	128	7	424	7

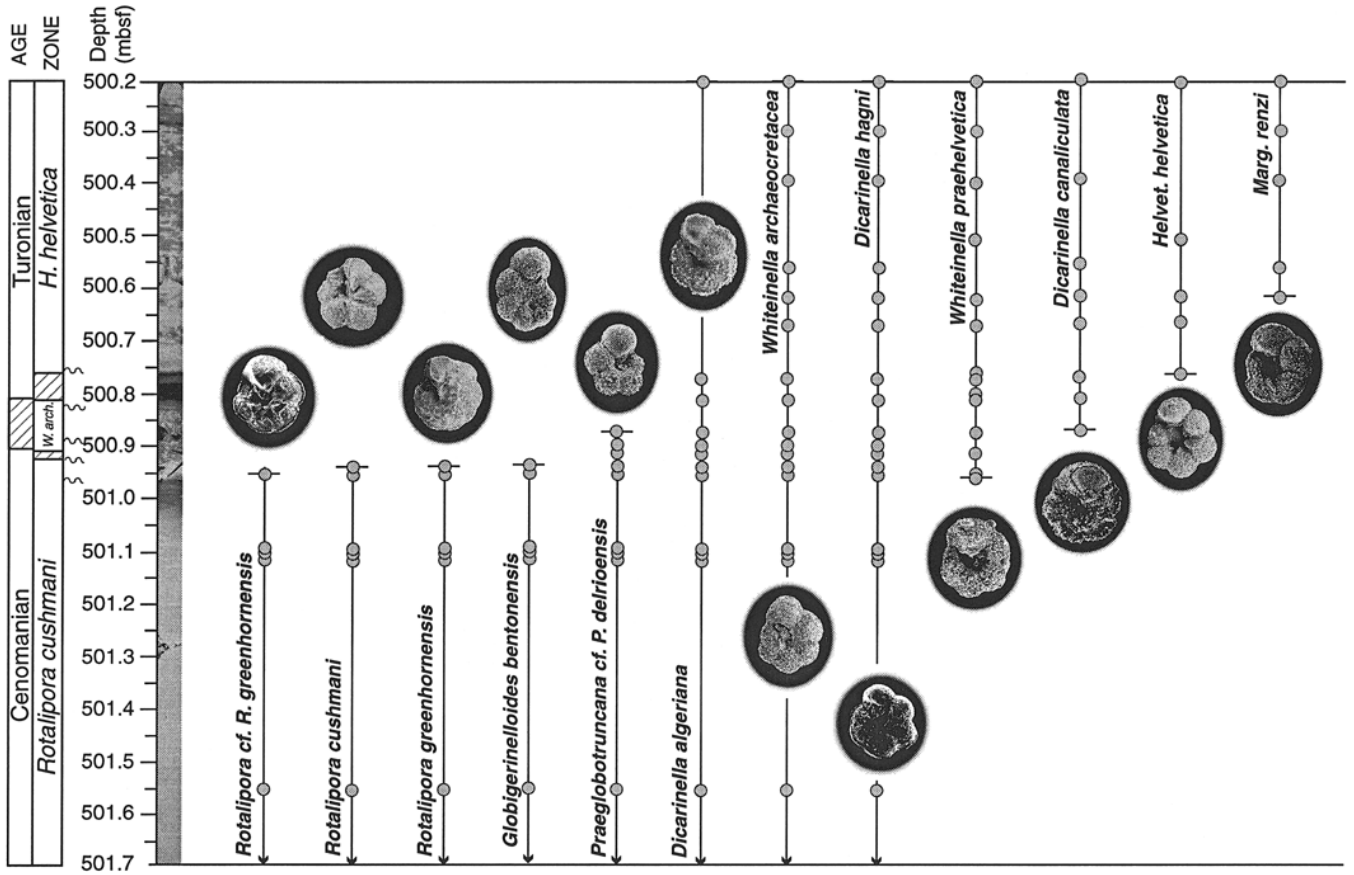

FIGURE 5. Distribution of select planktic foraminifera showing levels of their occurrences relative to Section 1050C-21R-1. Dots represent sample levels where each species has been identified.

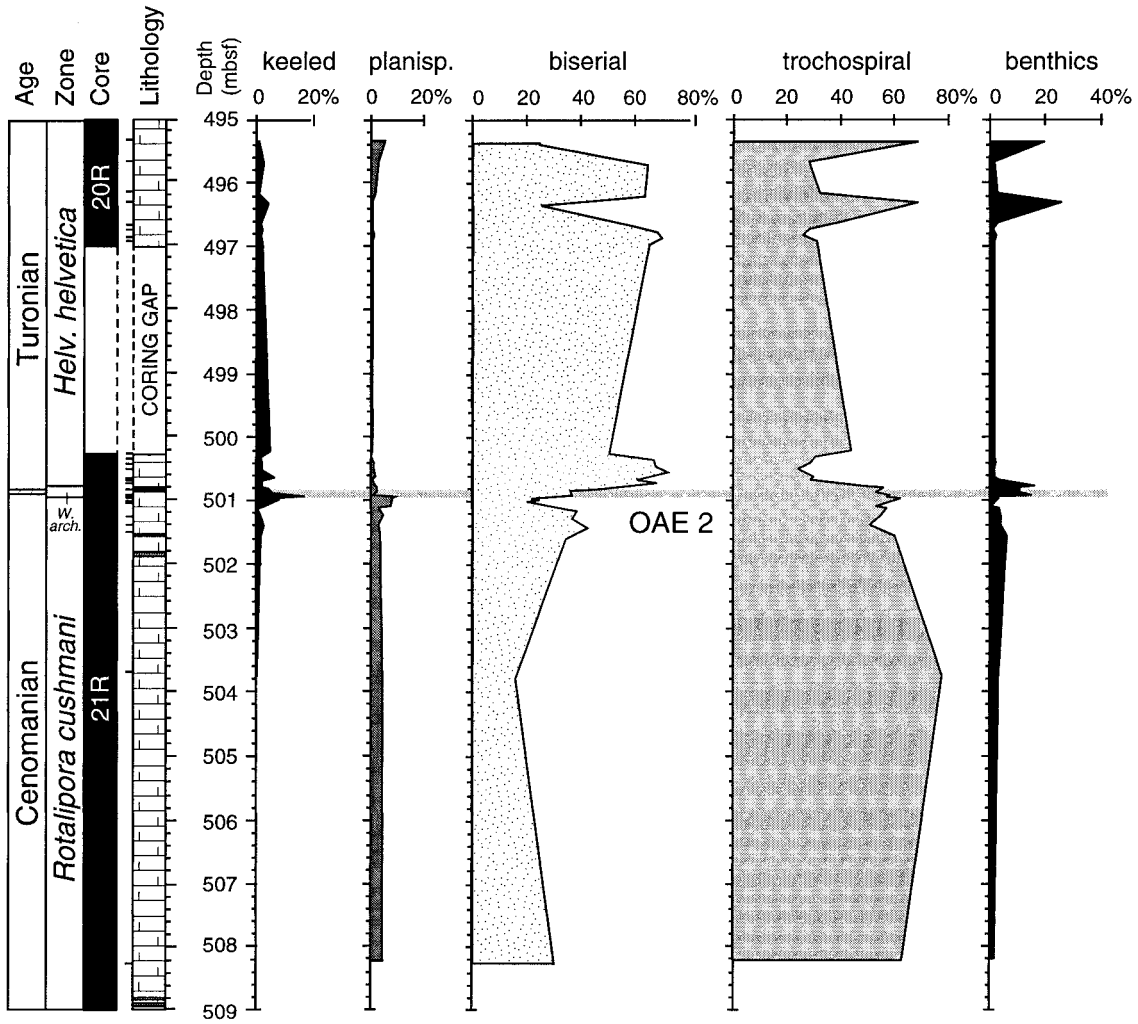

FIGURE 6. Abundance plots for planktic foraminifer morphotypes from the >63 μm fraction of samples from 495 to 510 mbsf in Hole 1050C. Tick marks on left side of lithology column represent sample levels. See text for listing of genera included in each morphotype category.

both the number of species and their relative abundances, while making no assumptions about an underlying distribution (Hayek and Buzas, 1997). Equitability was calculated as

$$E = e^{H(S)}/S$$

and measures how evenly the individuals are distributed among the species present in any given sample.

TABLE 2. Numerical and relative abundance data for planktic foraminifera from the >125 μm size fraction. See text for definitions of abundance and preservation categories.

HOLE 1050C	TOP DEPTH	ZONE	PRESERVATION	BENTHICS	UNKNOWN PLANKTICS	*Rotalipora* sp.	*Rotalipora* aff. *greenhornensis*	*Rotalipora cushmani*	*Rotalipora deekei*	*Rotalipora greenhornensis*	*Globigerinelloides bentonensis*	*Praeglobotruncana* cf. *delrioensis*	*Hedbergella delrioensis*	*Dicarinella algeriana*	*Dicarinella hagni*	*Dicarinella imbricata*	*Hedbergella planispira*	*Hedbergella* cf. *simplicissima*	*Heterohelix globulosa*	*Heterohelix moremani*	*Praeglobotruncana aumalensis*	*Praeglobotruncana gibba*	*Praeglobotruncana inornata*	*Praeglobotruncana stephani*	*Whiteinella aprica*	*Whiteinella archaeocretacea*	*Whiteinella baltica*	*Whiteinella buttonensis*	*Helvetoglobotruncana praehelvetica*	*Dicarinella canaliculata*	*Helvetoglobotruncana helvetica*	*Marginotruncana?* sp.	*Hedbergella holmdelensis*	*Marginotruncana renzi*	*Globigerinelloides* sp.	*Marginotruncana schneegansi*	TOTAL
21R-1, 0-1	500.20	*H. helvetica*	G	4	2								32	2	P	7	5	97	55	7	3	5	1	3	5	2	5	2	26	7	35			20		2	323
21R-1 10-11	500.30	*H. helvetica*	M	P									F	P	P	R		C	C	P		P		P	R	P	R	R	F		P	R		R	P	
21R-1, 20-21	500.40	*H. helvetica*	M	P									C		R	F		C	C	P	P			P	R	R	R	R	C	P	P	R		R	P	
21R-1, 31-34	500.51	*H. helvetica*	M	P									C	P	R	R	P	F	C	R		P		P	P	F	P	P	C		P	P		P	P	
21R-1, 42-43	500.62	*H. helvetica*	M	1	19								39	1	11	20	5	30	76	6	1	1	P	P	5	6	1	6	45	4	3	6		3	1		289
21R-1, 47-48	500.67	*H. helvetica*	M	1	13								55	5	27	20	5	28	40	4	P	1	6	1	2	10	6	6	59	7	4	7	2				308
21R-1, 56.5-57.5	500.77	*H. helvetica*	M	21	16				r				57	9	20	27	18	17	13	2	P	1	1	3	9	16	12	8	56	7	1	5					298
21R-1, 61-62	500.81	*W. archaeo.*	G	25	5			r			r		49	19	22	12	11	23	14	P	13	2	P	23	9	14	6	7	59	11							299
21R-1, 68-69	500.88	*W. archaeo.*	G	8	6					r	r	4	42	10	27	46	8	18	13	P	11	9	2	10	17	20	14	11	33	4							305
21R-1, 70-71	500.90	*W. archaeo.*	G	R								R	C	F	F	C		R	R		R	R	R	R	R	R	R	R	F								
21R-1, 72-73	500.92	*R. cushmani*	M	13	21			1		2	1	6	53	34	24	26	3	22	11	2	14	2	P	6	10	14	6	12	32								302
21R-1, 74-75	500.94	*R. cushmani*	M	3	10		9	6		7	18	1	60	22	2	13	1	46	29	7	35	1	3	7	3	3	14	1	2								300
21R-1, 75-76	500.95	*R. cushmani*	G	3	8		9	15	1	22	20	1	35	29	19	16	1	11	15	2	18	5	2	26	1	24	6	8	11								303
21R-1, 76.5-77.5	500.97	*R. cushmani*	G	2	16	2	4	9	P	11	13	12	36	30	22	13	6	27	5	3	11	9	2	30	1	28	4	5	9								308
21R-1, 81-82	501.01	*R. cushmani*	G	1	2		P	7		4	47	3	72	19	11	11	5	37	4	13	8	2		18		25	5	9									302
21R-1, 92-93	501.12	*R. cushmani*	M				R	R	P	R	F	R	A	F	R	R	P	C	R	R	R	P	P	F		P		R									
21R-1, 135-136	501.55	*R. cushmani*	M	5	17	2	3	4	P	11	22	7	118	10	3	5	2	17	10	19	8	6	1	20	1	3	1	7									297

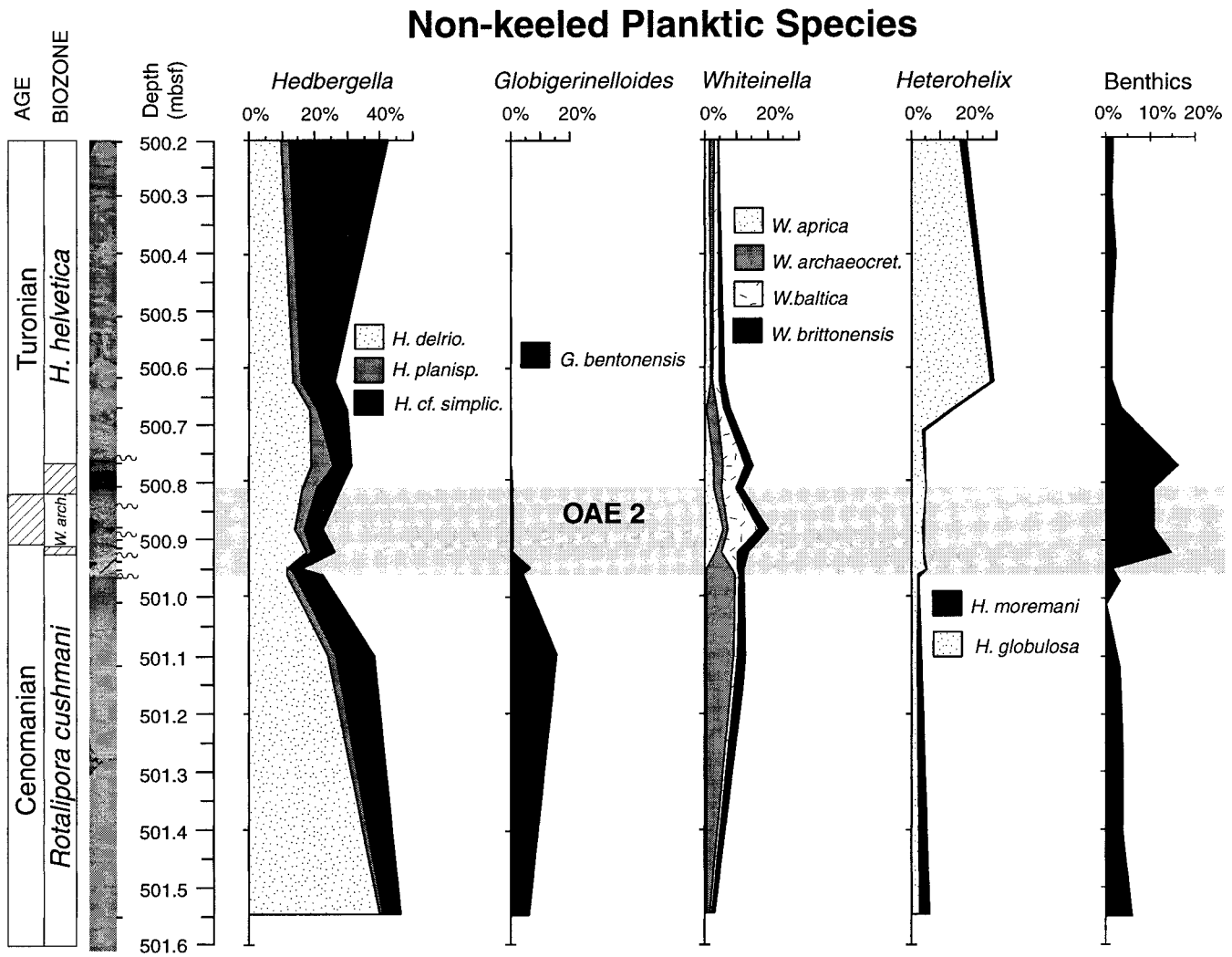

FIGURE 7. Abundance plots for non-keeled planktic foraminifer species from the >125 μm size fraction of samples from Section 1050C-21R-1. Tick marks on left side of lithology column represent sample levels.

These three indices are interrelated but are not redundant. Species richness could reflect the diversity of available habitats (*e.g.*, water column stratification, seasonality) as well as evolution (including extinction) or migration. H(S) diversity varies with species richness, but, for any given number of species (S), H(S) has a maximum value when all taxa are equally abundant and a minimum value when most of the individuals in a sample are represented by a single taxon. Equitability varies from 0.0 to 1.0 as the individuals present become more evenly distributed among the species present, and is independent of the number of species in a sample. This measure is difficult to uniquely interpret, but high E values are found in samples representing oligotrophic conditions (Nederbragt, 1991).

NANNOFOSSIL BIOSTRATIGRAPHY

Nannofossils were observed in smear slides prepared using the technique of Monechi and Thierstein (1985). All slides were observed in a transmitted light microscope at a magnification of 1000×. Detailed biostratigraphic investigations were carried out near the ends of species ranges between 500.81 and 500.99 mbsf. We compared the ranges of nannofossil species at Site 1050 with the results of Bralower (1988) who carried out detailed nannofossil biostratigraphy on the Cenomanian/Turonian boundary interval from numerous sites, including locations in the Western Interior Basin, Europe and several deep sea sites. Nannofossil biostratigraphy was also used to help determine the position of the Cenomanian/Turonian boundary.

STABLE ISOTOPIC METHODS

Monospecific and, where well-preserved specimens were rare, monogeneric assemblages of planktic foraminifera were picked for stable isotopic analyses. Typically at least one species of the biserial, trochospiral, and keeled morphotypes were picked from each sample (Table 3). Monogeneric benthic foraminifer assemblages were also picked from most samples. Multiple genera were combined only in samples where benthic foraminifera were very rare, and only taxa analyzed in other samples were included in the

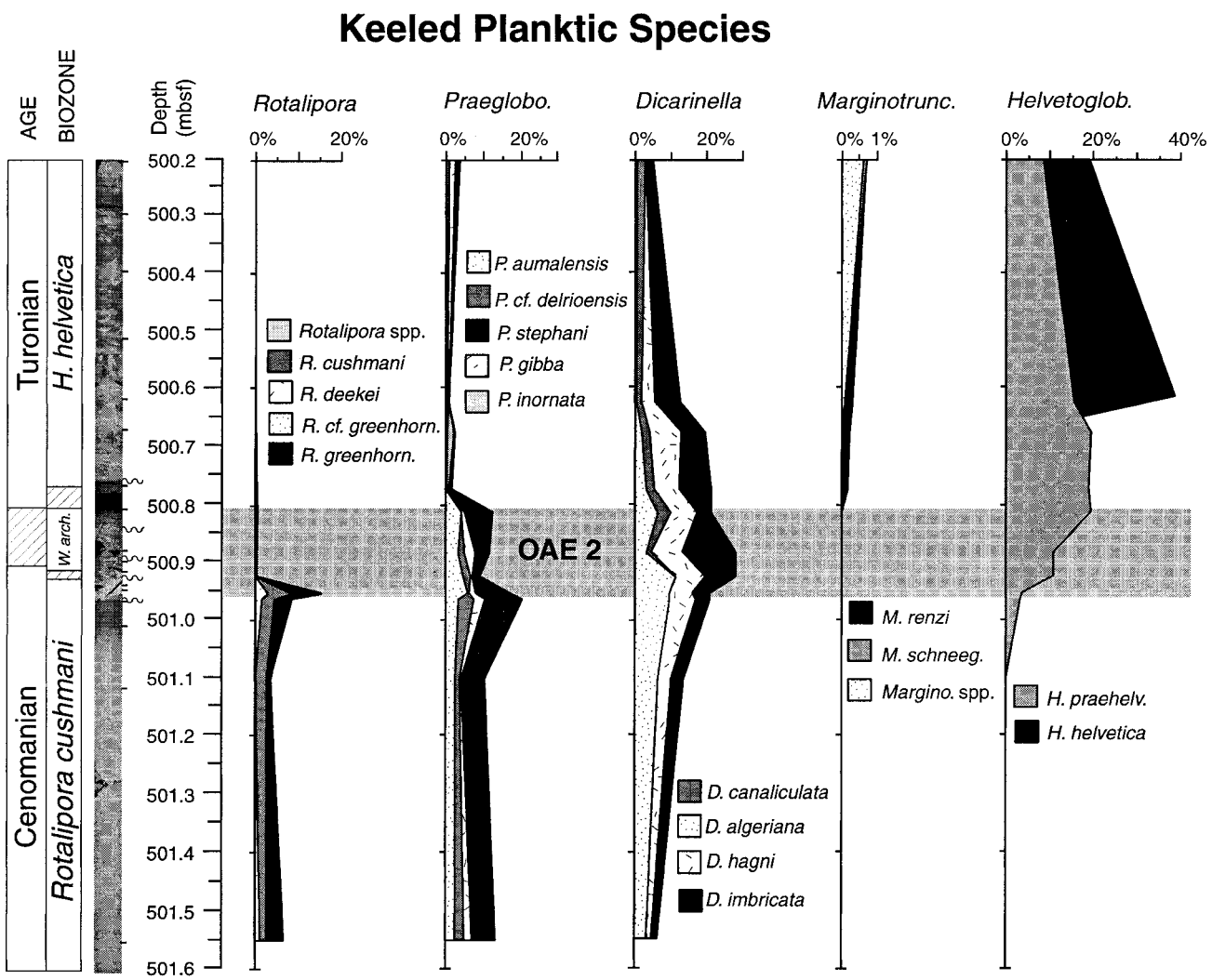

FIGURE 8. Abundance plots for non-keeled planktic foraminifer species from the >125 μm size fraction of samples from Section 1050C-21R-1. Tick marks on left side of lithology column represent sample levels.

combined analyses. Replicates were run on several samples to determine intra-sample variability. Moderately preserved samples with adhering chalky matrix were cleaned with a dissecting needle in an ultrasonic bath to minimize the potential contribution of non-foraminiferal carbonate to the stable isotopic signal. When necessary, some shells were broken open and cleaned to separate adhering matrix. Specimens that could not be freed of adherent matrix or that exhibited visible secondary calcite overgrowth were not analyzed.

Stable isotope analyses were performed using a Finnigan MAT 252 mass spectrometer with an on-line automated carbonate reaction Kiel device at Woods Hole Oceanographic Institution. Analytical precision based on repeated analysis of standards (NBS-19, Carrara marble, and B-1 marine carbonate) was better than 0.03‰ for $\delta^{13}C$ and 0.08‰ for $\delta^{18}O$. Sample values are reported relative to the Peedee belemnite (PDB) standard. Paleotemperatures were calculated using the equation of Erez and Luz (1983) and the standard mean ocean water (SMOW)/PDB conversion of −027‰ (Hut, 1987), and assuming $-1.2‰_{SMOW}$ for a non-glacial world (Shackleton and Kennett, 1975).

CARBON, SULFUR AND CARBONATE ANALYSES

Elemental analyses were performed on a Leco CS300 carbon/sulfur analyzer in the Biogeochemistry Laboratory at the University of Massachusetts. Total carbon and total sulfur analyses involved the combustion of 250 mg of raw, powdered samples. To determine the organic carbon content of samples, 250 mg of powdered sample were acidified with 1N hydrochloric acid for 48 hours to eliminate carbonate. Samples were then filtered with distilled deionized water and collected on a GFC sterile glass filter. Filtered samples were dried in a 50°C oven for 24 hours before analysis. The Leco CS300 was calibrated with both internal and commercial standards. Reproducibility for the analyses is 0.01% for carbon and 0.05% for sulfur. These data are reported in Table 4.

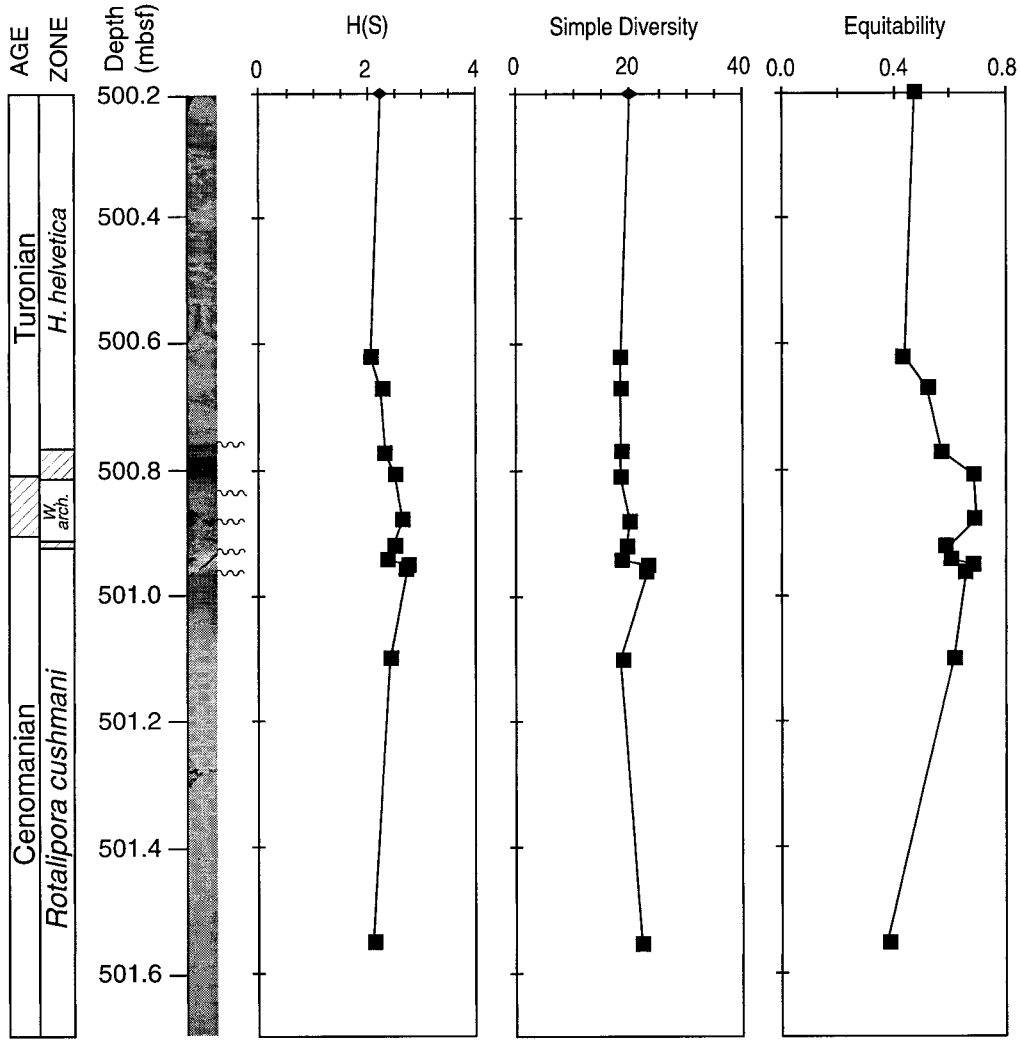

FIGURE 9. Simple species diversity, Shannon diversity, and equitability of planktic foraminifer assemblages from Section 1050C-21R-1. See text for explanation.

BIOSTRATIGRAPHIC RESULTS

FORAMINIFERAL DISTRIBUTIONS

The 15 m interval discussed in this study extends from the upper *R. cushmani* Zone, through the *W. archaeocretacea* Zone, and into the upper *H. helvetica* Zone. Foraminifera are abundant in all samples and their preservation ranges from good to moderate (Tables 1, 2). No radiolarians were encountered in the foraminifer samples and other biogenic constituents, such as ostracodes, fish teeth, and calcispheres, were rare to absent.

Biostratigraphic Summary

The *R. cushmani* Zone is ~19 m thick in Hole 1050C, but only the upper 9 m are included in this study. The top of this zone is marked by the extinction of the nominate species, which occurs at the contact between the white and gray marly debris flow bed at 500.93 mbsf (Fig. 3). Also disappearing at this level are *R. greenhornensis* and *Globigerinelloides bentonensis*. The last occurrences (LO) of *Rotalipora* aff. *R. greenhornensis* and *Rotalipora deekei* are within the top 3 cm of the zone (Fig. 5; Table 2). Coextinction of *R. greenhornensis* and *R. cushmani* has also been observed in the Pueblo, Colorado C/T section (Leckie, 1985) and the Bottaccione section of central Italy (Premoli Silva and Sliter, 1994), but *R. greenhornensis* consistently disappears at a lower level than *R. cushmani* in northern European sections (Jarvis and others, 1988). Just below the rotaliporid extinctions is the first occurrence (FO) of *Helvetoglobotruncana praehelvetica*, at 500.97 mbsf.

The few rotaliporids and globigerinelloidids that occur in the sample from 500.92 mbsf probably result from mixing across the lithologic boundary between the white and gray debris flow beds. Isolated specimens of *Rotalipora* and *G. bentonensis* occur up to 16 cm above this level, but these occurrences are considered the result of bioturbation and/or reworking as the color of the suspect specimens is different from the co-occurring assemblage.

The *Whiteinella archaeocretacea* Zone, which extends from the extinction of *R. cushmani* to the FO of *Helveto-*

TABLE 3. Oxygen and carbon isotope data for planktic and benthic foraminifera from Hole 1050C. All values are expressed in δ notation as per mil deviations from the Pee Dee Belemnite standard. Benthic species include *Gavelinella* sp., *Nuttalides* sp., and *Gyroidina globosa*.

Sample	MBSF	Species	$\delta^{13}C$	$\delta^{18}O$
20R-4, 29-32	495.34	*Nuttalides* sp.	2.056	−0.88
20R-4, 29-32	495.34	*Heterohelix moremani*	2.539	−1.158
20R-4, 29-32	495.34	*Marginotruncana pseudolinneiana*	2.845	−1.030
20R-4, 29-32	495.34	*Whiteinella baltica*	2.535	−1.578
20R-4, 61.5-62.5	495.67	*Heterohelix globulosa*	2.666	−1.819
20R-4, 61.5-62.5	495.67	*Praeglobotruncana gibba*	2.880	−1.890
20R-4, 61.5-62.5	495.67	*Helvetoglobotruncana helvetica*	2.919	−2.182
20R-4, 110-111	496.15	*Heterohelix globulosa*	2.648	−1.976
20R-4, 110-111	496.15	*Praeglobotruncana gibba*	2.753	−2.042
20R-4, 110-111	496.15	*Helvetoglobotruncana helvetica*	2.650	−2.115
20R-4, 120-121	496.30	*Marginotruncana pseudolinneiana*	2.863	−1.240
20R-4, 120-121	496.30	*Nuttalides* sp.	2.175	−0.776
20R-5, 7-8	496.62	*Helvetoglobotruncana helvetica*	2.838	−1.967
20R-5, 7-8	496.62	*Heterohelix globulosa*	2.660	−1.905
20R-5, 18-19	496.73	*Heterohelix globulosa*	2.796	−2.097
20R-5, 18-19	496.73	*Helvetoglobotruncana helvetica*	2.866	−2.149
20R-5, 27-28	496.82	*Heterohelix globulosa*	2.830	−2.103
20R-5, 27-28	496.82	*Praeglobotruncana gibba*	3.004	−2.226
20R-5, 37-38	496.92	*Heterohelix globulosa*	2.695	−2.065
20R-5, 37-38	496.92	*Praeglobotruncana gibba*	2.890	−2.045
20R-5, 37-38	496.92	*Helvetoglobotruncana helvetica*	2.933	−2.147
20R-5, 37-38	496.92	*Whiteinella brittonensis*	2.896	−2.148
20R-5, 40-42	496.95	*Helvetoglobotruncana helvetica*	2.731	−1.731
20R-5, 40-42	496.95	*Rotalipora gibba*	2.705	−1.698
20R-5, 40-42	496.95	*Marginotruncana marianosi*	2.618	−1.871
21R-1, 10-11	500.30	*Heterohelix globulosa*	2.583	−1.737
21R-1, 10-11	500.30	*Dicarinella hagni*	2.716	−1.920
21R-1, 10-11	500.30	*Whiteinella brittonensis*	2.720	−2.049
21R-1, 20-21	500.40	*Whiteinella archaeocretacea*	2.749	−1.672
21R-1, 20-21	500.40	*Gavelinella* sp.	1.977	−1.269
21R-1, 20-21	500.40	*Whiteinella archaeocretacea*	2.651	−1.618
21R-1, 20-21	500.40	*Dicarinella hagni*	2.686	−1.816
21R-1, 20-21	500.40	*Heterohelix globulosa*	2.540	−1.674
21R-1, 20-21	500.40	*Heterohelix moremani*	2.406	−1.478
21R-1, 20-21	500.40	*Dicarinella hagni*	2.792	−1.762
21R-1, 42-43	500.62	*Whiteinella brittonensis*	2.554	−2.017
21R-1, 42-43	500.62	*Gavelinella* sp.	1.817	−1.434
21R-1, 42-43	500.62	*Dicarinella hagni*	2.589	−1.928
21R-1, 42-43	500.62	*Heterohelix moremani*	2.426	−1.699
21R-1, 47-48	500.67	*Heterohelix moremani*	2.135	−1.959
21R-1, 47-48	500.67	*Heterohelix globulosa*	2.371	−1.981
21R-1, 47-48	500.67	*Cibicides* sp.	1.998	−1.148
21R-1, 47-48	500.67	*Whiteinella brittonensis*	2.536	−2.098
21R-1, 47-48	500.67	*Gavelinella* sp.	1.756	−1.362
21R-1, 47-48	500.67	*Dicarinella hagni*	2.577	−1.978
21R-1, 47-48	500.67	*Whiteinella archaeocretacea*	2.537	−2.267
21R-1, 47-48	500.67	*Dicarinella hagni*	2.625	−2.074
21R-1, 47-48	500.67	*Helvetoglobotruncana praehelvetica*	2.518	−2.058
21R-1, 56.5-57.5	500.77	*Whiteinella brittonensis*	2.396	−1.922
21R-1, 56.5-57.5	500.77	*Gavelinella* sp.	1.685	−1.150
21R-1, 56.5-57.5	500.77	*Dicarinella hagni*	2.605	−1.789
21R-1, 56.5-57.5	500.77	*Heterohelix moremani*	2.433	−1.666
21R-1, 60-61	500.80	*Whiteinella brittonensis*	2.546	−2.207
21R-1, 60-61	500.80	*Gavelinelia* sp.	1.791	−1.432
21R-1, 60-61	500.80	*Dicarinella hagni*	2.625	−2.061
21R-1, 60-61	500.80	*Heterohelix moremani*	2.384	−1.965
21R-1, 61-62	500.81	*Whiteinella brittonensis*	2.606	−1.854
21R-1, 61-62	500.81	*Gavelinella* sp.	2.037	−1.449
21R-1, 61-62	500.81	*Dicarinella hagni*	2.680	−1.892
21R-1, 61-62	500.81	*Heterohelix moremani*	2.405	−1.789
21R-1, 68-69	500.88	*Heterohelix globulosa*	2.508	−1.855
21R-1, 68-69	500.88	*Gavelinella* sp.	2.380	−1.486
21R-1, 68-69	500.88	*Heterohelix moremani*	2.325	−1.748
21R-1, 68-69	500.88	*Dicarinella hagni*	2.768	−1.963
21R-1, 68-69	500.88	*Whiteinella archaeocretacea*	2.743	−2.048
21R-1, 68-69	500.88	*Helvetoglobotruncana praehelvetica*	2.902	−2.243
21R-1, 70.5-71.5	500.91	*Dicarinella algeriana*	2.848	−1.863
21R-1, 70.5-71.5	500.91	*Praeglobotruncana stephani*	2.794	−1.891
21R-1, 70.5-71.5	500.91	*Whiteinella aprica*	2.667	−1.555

TABLE 3. Continued.

Sample	MBSF	Species	$\delta^{13}C$	$\delta^{18}O$
21R-1, 70.5-71.5	500.91	*Gavelinella* sp.	2.513	−1.613
21R-1, 72-73	500.92	*Whiteinella brittonensis*	2.815	−2.016
21R-1, 72-73	500.92	*Gavelinella* sp.	2.454	−1.581
21R-1, 72-73	500.92	*Rotalipora greenhornensis*	2.723	−1.984
21R-1, 72.5-73.5	500.93	*Rotalipora cushmani*	2.553	−1.354
21R-1, 72.5-73.5	500.93	*Rotalipora greenhornensis*	2.583	−1.654
21R-1, 74.5-75.5	500.95	*Rotalipora cushmani*	2.474	−1.78
21R-1, 74.5-75.5	500.95	*Rotalipora greenhornensis*	2.694	−1.592
21R-1, 74.5-75.5	500.95	*Whiteinella archaeocretacea*	2.712	−1.64
21R-1, 74.5-75.5	500.95	*Gavelinella* sp.	1.900	−0.822
21R-1, 75-76	500.95	*Whiteinella archaeocretacea*	2.651	−1.857
21R-1, 75-76	500.95	*Gavelinella* sp.	1.923	−1.087
21R-1, 75-76	500.95	*Rotalipora greenhornensis*	2.621	−1.595
21R-1, 75-76	500.95	*Heterohelix moremani*	2.603	−1.955
21R-1, 76.5-77.5	500.97	*Whiteinella archaeocretacea*	2.758	−2.094
21R-1, 76.5-77.5	500.97	*Gavelinella* sp.	1.644	−1.291
21R-1, 76.5-77.5	500.97	*Gavelinella* sp.	1.790	−1.075
21R-1, 76.5-77.5	500.97	*Heterohelix moremani*	2.207	−2.013
21R-1, 76.5-77.5	500.97	*Whiteinella archaeocretacea*	2.660	−2.181
21R-1, 76.5-77.5	500.97	*Rotalipora cushmani*	2.311	−1.649
21R-1, 76.5-77.5	500.97	*Rotalipora greenhornensis*	2.539	−1.719
21R-1, 81-82	501.01	*Whiteinella brittonensis*	2.456	−2.617
21R-1, 81-82	501.01	*Gavelinella* sp.	1.567	−0.812
21R-1, 81-82	501.01	*Rotalipora greenhornensis*	2.448	−1.821
21R-1, 81-82	501.01	*Heterohelix moremani*	2.417	−2.053
21R-1, 92-93	501.12	*Whiteinella baltica*	2.582	−1.621
21R-1, 92-93	501.12	*Gavelinella* sp.	2.227	−1.184
21R-1, 92-93	501.12	*Whiteinella baltica*	2.574	−1.963
21R-1, 92-93	501.12	*Rotalipora cushmani*	2.381	−1.475
21R-1, 92-93	501.12	*Heterohelix moremani*	2.265	−1.931
21R-1, 92-93	501.12	*Rotalipora greenhornensis*	2.496	−1.432
21R-1, 92-93	501.12	*Heterohelix moremani*	2.414	−1.807
21R-1, 120-121	501.40	*Whiteinella brittonensis*	2.534	−2.154
21R-1, 120-121	501.40	*Gavelinella* sp.	1.854	−0.831
21R-1, 120-121	501.40	*Rotalipora greenhornensis*	2.527	−1.465
21R-1, 135-136	501.55	*Whiteinella archaeocretacea*	2.639	−2.120
21R-1, 135-136	501.55	*Rotalipora greenhornensis*	2.572	−1.565
21R-1, 135-136	501.55	*Heterohelix moremani*	2.460	−1.776
21R-1, 135-136	501.55	*Rotalipora cushmani*	2.472	−1.555
21R-3, 56-59	503.76	*Whiteinella archaeocretacea*	2.405	−2.127
21R-3, 56-59	503.76	*Rotalipora cushmani*	2.113	−1.826
21R-3, 56-59	503.76	*Heterohelix moremani*	2.060	−1.692
21R-4, 63-66	505.33	*Rotalipora greenhornensis*	2.189	−1.680
21R-4, 63-66	505.33	*Heterohelix moremani*	2.154	−1.799
21R-4, 63-66	505.33	*Whiteinella baltica*	2.372	−1.997
21R-4, 63-66	505.33	*Gyroidina globosa*	1.269	−0.814
21R-4, 129-132	505.99	*Whiteinella archaeocretacea*	2.378	−2.081
21R-4, 129-132	505.99	*Gavelinella* sp.	1.503	−1.137
21R-4, 129-132	505.99	*Rotalipora cushmani*	2.109	−1.809
21R-4, 129-132	505.99	*Heterohelix moremani*	2.098	−1.830
21R-6, 54-57	508.24	*Whiteinella baltica*	2.391	−2.364
21R-6, 54-57	508.24	*Rotalipora cushmani*	2.127	−1.912
21R-6, 54-57	508.24	*Heterohelix moremani*	2.113	−2.270
21R-7, 45-46	508.75	*Rotalipora greenhornensis*	2.232	−1.517
21R-7, 45-46	508.75	*Heterohelix moremani*	2.015	−1.755
21R-7, 45-46	508.75	*Gyroidina globosa*	1.837	−0.596
21R-7, 105-108	509.25	*Rotalipora cushmani*	2.045	−2.777
21R-7, 105-108	509.25	*Heterohelix globulosa*	1.693	−3.455
21R-7, 105-108	509.25	*Rotalipora greenhornensis*	2.115	−2.584
21R-7, 105-108	509.25	*Whiteinella archaeocretacea*	2.441	−3.294
21R-CC, 27-31	509.78	*Rotalipora gibba*	2.688	−2.035
21R-CC, 27-31	509.78	*Rotalipora greenhornensis*	2.224	−1.718
21R-CC, 27-31	509.78	*Rotalipora cushmani*	2.255	−2.124
21R-CC, 27-31	509.78	*Heterohelix globulosa*	2.472	−2.054

TABLE 4. Percentages of inorganic carbon, carbonate, total organic carbon, ant total sulfer for upper Cenomanian-lower Turonian samples from Hole 1050C. Values are based on averages from two analyses per sample except for value reported with an asterisk and are expressed as weight percent.

Hole 1050C	Top depth	% Inorganic carbon	% Carbonate	% Tot. organic carbon	% Total sulfer
20R-4, 29-32	495.34	9.509	79.244	0.008	0.068
20R-5, 37-38	496.92	8.209	68.408	0.034	0.057
21R-1, 10-11	500.30	10.019	83.488	0.010	0.060
21R-1, 47-48	500.67	8.330	69.421	0.025	0.078
21R-1, 56-57	500.76	6.753	56.276	0.008	0.088
21R-1, 60-61	500.80	1.676	13.963	0.010	0.083
21R-1, 81-82	501.10	7.611	63.426	0.015	0.062
21R-1, 120-121	501.40	10.594	88.279	0.012	0.035
21R-2, 99-102	502.69	10.123	84.358	0.024	0.062
21R-3, 56-59	503.76	10.095	84.121	0.029	0.064
21R-4, 63-66	505.33	9.542	79.517	0.014	0.051
21R-6, 54-57	508.24	9.968	83.069	0.024*	0.054
21R-7, 51-52	508.81	9.201	76.674	0.663	0.546

globotruncana helvetica (Bolli, 1966; Caron, 1985), ranges from 500.93 mbsf to 500.77 mbsf. The FO of *Dicarinella canaliculata*, a latest Cenomanian-earliest Turonian marker (Robaszynski and others, 1979), lies in the lower part of this zone at 500.88 mbsf. Within 11 cm above this level is the FO of an unidentified form of *Marginotruncana*. The FOs of other early Turonian markers, *Marginotruncana renzi* and *M. schneegansi*, lie at 500.62 and 500.20 mbsf, respectively.

Morphogroup Abundance Patterns

Results from counts of planktic foraminiferal and benthic morphotypes from the >63 μm size fraction are presented in Figure 6. One of the most noticeable population changes is a shift from trochospiral dominated assemblages in the *R. cushmani* Zone and lower *W. archaeocretacea* Zone to biserial dominated assemblages beginning in the upper *W. archaeocretacea* Zone at 500.67 mbsf. This "*Heterohelix* shift" was recorded slightly lower, in the uppermost Cenomanian, at sites in the southwest Western Interior (USA) (Leckie and others, 1998) and at several Tethyan land and deep-sea sections (Nederbragt and others, 1998).

Other significant changes in the foraminifer populations occur near or at the level of the rotaliporid extinction. Below 500.97 mbsf keeled taxa range from 0.6 to 2.7% of the total assemblage, but their abundance increases to 8% and then 18% within the uppermost 5 cm of the *R. cushmani* Zone, and then drops to between 1 and 7% within the *W. archaeocretacea* and *H. helvetica* Zones. The planispiral morphogroup ranges between 2.7 and 4.7% of the assemblages below 500.01 mbsf, increases to 7 to 9% to the top of the *R. cushmani* Zone, and then drops to between 0.3 and 2.3% in the *W. archaeocretacea* Zone. A rare, small form of *Globigerinelloides* persists through the *W. archaeocretacea* Zone following the *G. bentonensis* extinction. The increase in *Schackoina* observed below the Bonarelli Event in Italy (Premoli Silva and others, 1999) was not observed at Site 1050, as this taxon was consistently too rare to be included in the planispiral abundance counts.

Benthic foraminifera also change at the level of the rotaliporid extinction. Whereas assemblages in the *R. cushmani* Zone range from between 0.3 and 6%, samples from the lowermost 15 cm of the *W. archaeocretacea* Zone yield benthic abundance between 10 and 16%. This change occurs across the contact between the white and gray colored debris flow beds at 500.93 mbsf (Fig. 3).

Species Abundance Patterns

The patterns of change in species abundance for the >125 μm size fraction in Section 1050C-21R-1 are summarized in Figure 7 for keeled species and Figure 8 for non-keeled species. As shown in the morphogroup plots, the major change among the non-keeled species is the *Heterohelix* shift at 500.62 mbsf. Whereas *H. moremani* is the dominant heterohelicid below the rotaliporid extinction, this species is outnumbered by *H. globulosa* above that level. This switch in dominance was also observed across the CTBI by Nederbragt and others (1998). At this level there is also a gradual replacement of *Hedbergella delrioensis* by *H.* cf. *H. simplicissima* and diminishing abundance of *W. archaeocretacea*.

Keeled species generally comprise about one-third of the total planktic foraminiferal assemblages across the CTBI. In the upper *R. cushmani* Zone, *R.* aff. *R. greenhornensis*, *R. greenhornensis*, and *R. cushmani* are about equal in abundance, mostly varying between 1 and 5% of the assemblage, while *R. deekei* is very rare and sporadic in its occurrence. Praeglobotruncanids are more common than rotaliporids, ranging between 10 and 21% of the assemblage, with *P. stephani* as the most common species. Dicarinellids become the dominant keeled group with as much as 28% abundance at the level of the rotaliporid extinction, but then diminish to 5% abundance at the base of the *H. helvetica* Zone. Within the *W. archaeocretacea* Zone the helvetoglobotruncanids take over as the dominant keeled taxon, comprising 15 to 20% of the early Turonian assemblages. Marginotruncanids are consistently rare after their first occurrence, comprising less than 1% of the assemblages.

Species Diversity and Equitability

The planktic foraminiferal diversity and equitability plots show relatively minor change through the C/T core-section (Fig. 9). Species richness varies from 18 to 23 species in the *R. cushmani* Zone, with maximum diversity occurring immediately below the LO of *Rotalipora*. In the *W. archaeocretacea* Zone species richness varies between 18 and 20 species. H(S) values show a similar trend, with a maximum value in the uppermost *R. cushmani* Zone.

Equitability is highest in the uppermost *R. cushmani* Zone and lower *W. archaeocretacea* Zone with values ranging from 0.60 to 0.69. The low value in the assemblage at 501.55 mbsf reflects dominance in the sample of hedbergellids, and the diminishing values in the upper *W. archaeocretacea* Zone reflect increasing dominance by heterohelicids.

PLACEMENT OF THE CENOMANIAN/TURONIAN BOUNDARY

Although planktic foraminiferal ranges help constrain placement of the C/T boundary to between the LO of ro-

taliporids at 500.93 mbsf and the FO of *H. helvetica* at 500.77 mbsf (Fig. 5), the location of the boundary can be better resolved using calcareous nannofossil biostratigraphy. Nannofossils are abundant in all Section 1050C-21R-1 samples except clay clasts at 500.94 mbsf and 500.87 mbsf in which they are virtually barren. Preservation is moderate to good. Samples from 501.00–500.90 mbsf contain a typical late Cenomanian assemblage, including *Axopodorhabdus albianus*, *Cretarhabdus loriei*, *Corollithion achylosum*, *C. kennedyi*, *Microstaurus chiastius*, *Lithraphidites acutum* and *Rhagodiscus asper*. The last occurrences of several prominent markers, including *A. albianus*, *C. kennedyi*, *M. chiastius, L. acutum* and *R. asper*, lie between 500.90 and 500.81 mbsf. Based on these ranges, the interval below 500.90 mbsf lies in the *Axopodorhabdus albianus* Zone of Bralower (1988) (Fig. 3). The sample at 500.81 lies within the *Eprolithus floralis* Zone. Although the lack of fossiliferous samples between these levels prevents firm conclusions from being drawn, the nannofossil ranges suggest an unconformity between 500.90 and 500.81 mbsf, which includes the *Parhabdolithus* (*Rhagodiscus*) *asper* Zone and the Cenomanian/Turonian boundary. The first occurrence of *Quadrum gartneri*, a marker which has been used to define the base of Zone CC11 and the Cenomanian/Turonian boundary by Sissingh (1977), lies at 500.90 mbsf. However, several authors (e.g., Bralower [1988]) have shown that this species ranges down into the upper Cenomanian. The lack of *Eprolithus octopetalus*, *E. eptapetalus* and the presence of *C. achylosum* at 500.81 mbsf indicates that this level lies in the earliest Turonian (Bralower and Bergen, 1998).

In the Bottaccione section, 4 m of the *W. archaeocretacea* Zone are placed in the Cenomanian and 2 m are placed in the Turonian (Premoli Silva and Sliter, 1994). Assuming a sedimentation rate of 8.14 m/m.y. across the CTBI (*ibid.*) the duration of the *Whiteinella archaeocretacea* Zone is estimated as ~740 k.y., with ~490 k.y. in the Cenomanian and ~250 k.y. in the Turonian. In the Pueblo, Colorado section the *W. archaeocretacea* Zone has a similar stratigraphic distribution as at the Bottaccione section, with two-thirds of the zone in Cenomanian sediments and one-third in Turonian sediments (Leckie, 1985). Comparison with these sections indicates that as much as 77%, or ~380,000 years, of the Cenomanian portion of the *W. archaeocretacea* Zone is missing at Site 1050.

Multiple diastems at several lithologic breaks in Section 1050C-21R-1 probably account for the missing time in the *W. archaeocretacea* Zone. One possible location of a diastem is the erosional contact between white (Core 21R-1, 73-76.5 cm) and gray (Core 21R-1, 63-73 cm) clay clast-bearing sediments at 500.93 mbsf (Fig. 3). These have been interpreted as debris flow units (Norris, and others, 1998). The abrupt increase in percent benthic foraminifera, glauconite, and fish debris, oxygen and carbon isotope shifts (see below), and LOs of rotaliporids and *G. bentonensis* at this level are consistent with placement of a disconformity at this level. Another layer rich in glauconite and fish debris occurs within the gray clast-bearing unit in Core 21R-1, 68–69 cm (500.88–500.89 mbsf). This gray, clast-bearing debris flow unit may actually represent two events as supported by the additional observation that the clay clasts in the interval 500.93 to 500.89 are flattened and have rinds of white chalk, while the clay clasts in the interval 500.88 to 500.83 are rounded and lack the white chalk rinds. Therefore, two additional possibilities for diastems are within the gray clast-bearing unit (~500.88 mbsf) and at the top (500.83 mbsf). We interpret the glauconite and fish-debris-bearing layers at 500.93 and 500.88 mbsf to represent transgressive surfaces marked by erosion and condensed sedimentation. Sediment starvation due to transgression, coupled with bioturbation, bottom current scour, and downslope reworking of clay clasts from a local source, all contribute to the sedimentologic complexity of the white and gray clast-bearing units.

The clay clasts within Section 1050C-21R-1 were interpreted as rip-ups that were redeposited in a debris flow (Norris and others, 1998). X-ray diffraction, microprobe, and stereomicroscopic study of the clay clasts during the present study revealed that the clasts are entirely composed of magnesium-rich smectite and are devoid of microfossils. The Mg enrichment of the smectite and observations of crystalline ghosts with the clasts suggest that the clay is the alteration product of a tephra layer(s) that was deposited in a marine environment. Absence of shallow water benthic foraminifera from the debris flow interval indicates that they resulted from sediment slumping nearby rather than higher up the continental slope. The angularity of the clay clasts also supports this interpretation. Bioturbation may have also contributed to the fragmentation of the originally continuous tephra layer(s), and/or to the mixing of clay clasts within the putative debris flow units. While it seems unlikely that the two or three debris flows should be separated by a significant amount of time, the bio- and chemostratigraphic changes and comparison with other stratigraphies suggest that the total duration of diastems separating the slumps may be as much as 0.5 m.y.

STABLE ISOTOPIC RESULTS

Isotopic Preservation

Planktic foraminifer preservation of samples analyzed for stable isotopic study range from good to moderate based on stereomicroscope observation (Table 2). All specimens appear opaque because of shell recrystallization, and some specimens show a small to moderate amount of calcite encrustation.

To determine the degree of shell recrystallization and calcite overgrowth in the studied interval we broke open the shells of *H. globulosa* from samples representing the range of preservation quality and compared the shell ultrastructure and the wall textures of the chamber interiors. This species was selected for comparison because its thin shell wall is more susceptible to diagenetic alteration.

Calcite replacement and secondary calcite overgrowth are apparent on all specimens observed. Specimens with the least amount of shell recrystallization and calcite overgrowth occur in the most clay-rich layers and show faint traces of primary layering in the shell wall (Fig. 10a). Significant calcite infilling was observed in some samples from the most carbonate-rich intervals. The largest of the observed overgrowths partially fill the chamber interiors (e.g., Fig. 10b). Such specimens were excluded from our stable isotopic study.

The primary $\delta^{18}O$ ratios of biogenic calcite can be sub-

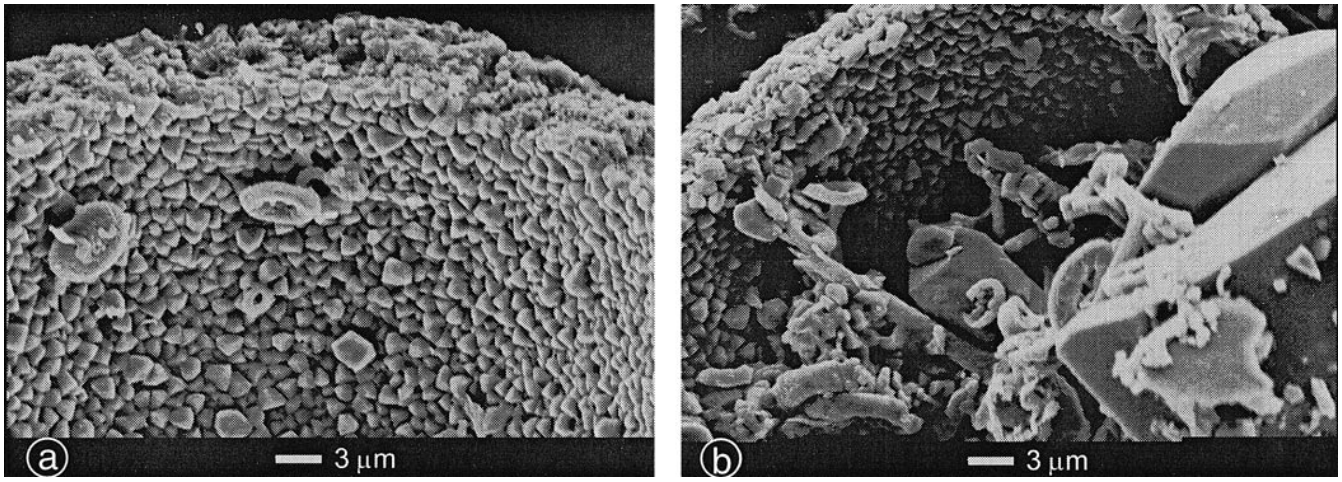

FIGURE 10. Scanning Electron Micrograph images of the chamber interior of Heterohelix globulosa showing wall texture preservation and degree of secondary calcite infilling. (a) Specimen from 1050C-21R-1, 76.5 cm showing significant chamber wall recrystallization but no test infilling. (b) Specimen from 1050C-21R-1, 120 cm showing significant chamber wall recrystallization and moderate infilling of secondary calcite. Specimens with such infilling were not selected for stable isotopic analysis.

stantially affected by dissolution and reprecipitation if the surrounding pore waters have different isotopic compositions and temperatures than the ambient water in which the organism grew (Killingley, 1983). On the other hand, the original $\delta^{13}C$ ratios are little affected by such replacement processes in sediments with a low total organic carbon content since the largest carbon reservoir is in the biogenic carbonate pool (Scholle and Arthur, 1980). We do not consider diagenesis to have significantly changed the original isotopic composition of the foraminifera included in this study since there is no systematic offset between samples with moderate vs. good preservation and because there are consistent offsets between the interspecies isotopic ratios (see below).

Carbon Isotopes

The most enriched benthic $\delta^{13}C$ values of the studied interval occur in samples that straddle the white and gray debris flow beds (Figs. 3, 11, 12). Below this level, from 509.00 to 501.25 mbsf, benthic foraminifer values range between 1.27 and 1.85‰, they increase to 2.23‰ at 501.12 mbsf, then decrease to 1.57‰ at 501.01 mbsf. From the base to the top of the white debris flow bed there is a 0.75‰ increase in $\delta^{13}C$ values that leads to a peak value of 2.45‰ in the sample that contains the LO of *Rotalipora*. The next sample higher, which is from the base of the gray debris flow, yields an enriched benthic $\delta^{13}C$ value of 2.38‰ (Fig. 12). This is followed by a gradual decrease to 1.69‰ at 500.77 mbsf, and then a gradual increase to slightly higher values in the upper *H. helvetica* Zone.

Planktic foraminifer $\delta^{13}C$ values show little change in the *R. cushmani* Zone below 500.97 mbsf. Within this interval *Whiteinella* spp. yields the most positive values among the species analyzed, varying between 2.37 and 2.58‰, whereas rotaliporid and heterohelicid $\delta^{13}C$ values are consistently more negative than whiteinellids by ~0.3‰. Beginning at 500.97 mbsf, the planktic species all show an ~0.4‰ $\delta^{13}C$ enrichment that parallels the more dramatic benthic $\delta^{13}C$ increase across the debris flow beds, and the differences between rotaliporid and whiteinellid values narrows to less than 0.1‰. At the base of the gray debris flow bed *Helvetoglobotruncana praehelvetica* yields a peak $\delta^{13}C$ value of 2.90‰ (Fig. 12). From this level through the top of the core-section *D. hagni* plots ~0.1–0.2‰ more positive than *Whiteinella* spp., first decreasing to 2.56‰ and then increasing to 2.79‰. In nearly all of these samples *H. globulosa* and *H. moremani* are more negative in their $\delta^{13}C$ composition than *D. hagni* by 0.2 to 0.5‰. Notably, *H. moremani* plots close to or more negative than corresponding benthic $\delta^{13}C$ values in several samples.

In the upper *H. helvetica* Zone the keeled species *Praeglobotruncana* spp. and *Marginotruncana* spp. yield the most positive $\delta^{13}C$ values, ranging between 2.71 and 2.88‰. *Heterohelix globulosa* is more negative than these values by 0.2 to 0.3‰.

The vertical $\delta^{13}C$ gradient between benthic and the most positive planktic foraminifera ranges from 0.6 to 0.8‰ in most upper Cenomanian and lower Turonian samples. The smallest $\delta^{13}C$ gradient of 0.37‰ occurs in the sample bearing the LO of *Rotalipora*.

Oxygen Isotopes

Benthic foraminifer $\delta^{18}O$ values generally vary between −0.6 and −0.9‰ in most of the upper Cenomanian and lower Turonian samples (Figs. 11, 12). As with the benthic $\delta^{13}C$ values, the most dramatic $\delta^{18}O$ change occurs in samples ranging from the uppermost *R. cushmani* Zone to the lower *W. archaeocretacea* Zone. Beginning at 501.12 mbsf benthic $\delta^{18}O$ values decrease by 0.76‰ to a minimum value of −1.58‰ at the top of the white debris flow bed where *Rotalipora* has its last occurrence (Fig. 3). The benthic values gradually increase by ~0.8‰ into the upper *H. helvetica* Zone.

The lowermost sample in the sequence produces the most negative planktic foraminifer $\delta^{18}O$ values, with *H. globulosa* yielding −3.46‰, *Whiteinella* spp. yielding −3.29‰, and

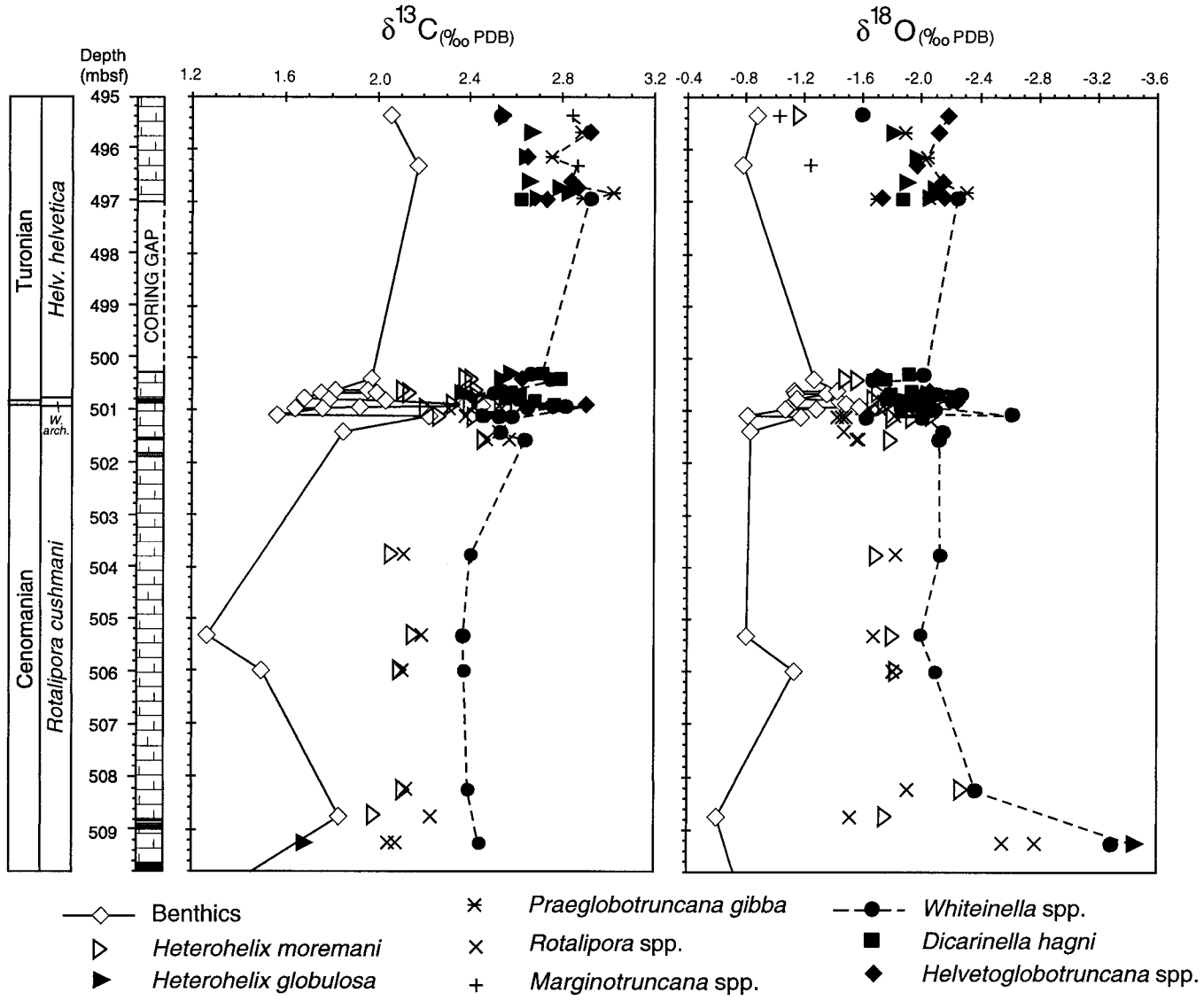

FIGURE 11. Oxygen and carbon isotope data for benthic and planktic foraminifer from 495–510 mbsf of Hole 1050C relative to the lithostratigraphy. Lithologic symbols are for chalk (horizontal lines with vertical bars) and dark, clay-rich layers (black horizontal bands).

Rotalipora spp. ranging between −2.78 and −2.55‰. In nearly all other Cenomanian and Turonian samples where it occurs, *Whiteinella* spp. has the most depleted $\delta^{18}O$ values, generally ranging between −1.8 and −2.3‰. Between 501.12 and 500.80 mbsf, whiteinellid $\delta^{18}O$ values generally parallel the $\delta^{18}O$ shift observed for benthic foraminifera, but the magnitude of change (~0.2‰) is insignificant in comparison.

Rotalipora cushmani and *R. greenhornensis* yield the most positive $\delta^{18}O$ values and plot within 0.05‰ of each other in most samples in which both species were analyzed. Relative to the whiteinellids, rotaliporids are 0.3 to 0.5‰ more enriched in $\delta^{18}O$ in a majority of the samples, but the $\delta^{18}O$ values of rotaliporids are about the same as those of whiteinellids at the level of the rotaliporid extinction.

Heterohelicid $\delta^{18}O$ values are intermediate to those of rotaliporids and whiteinellids in most samples from the *R. cushmani* Zone, and consistently higher than the most depleted planktic species above the rotaliporid extinction. In several samples *H. moremani* $\delta^{18}O$ values are halfway between the benthic and most depleted planktic species $\delta^{18}O$ compositions. Where both species were analyzed *H. moremani* has higher $\delta^{18}O$ values than *H. globulosa* by up to 0.32‰.

In the Turonian section the $\delta^{18}O$ composition of *Dicarinella hagni* typically lies within 0.1‰ of the whiteinellid values, but is as much as 0.3‰ more enriched than whiteinellids in several samples. Helvetoglobotruncanids are more depleted in $\delta^{18}O$ than other species from the same sample, and generally range between −1.90 and −2.20‰ within the *H. helvetica* Zone. On the other hand, $\delta^{18}O$ values of marginotruncanids lie closer to benthic $\delta^{18}O$ values than to the helvetoglobotruncanids. Praeglobotruncanids mostly lie within 0.1‰ of *H. globulosa* $\delta^{18}O$ values where both species were analyzed.

The vertical $\delta^{18}O$ gradient ranges between 0.8 and 1.3‰

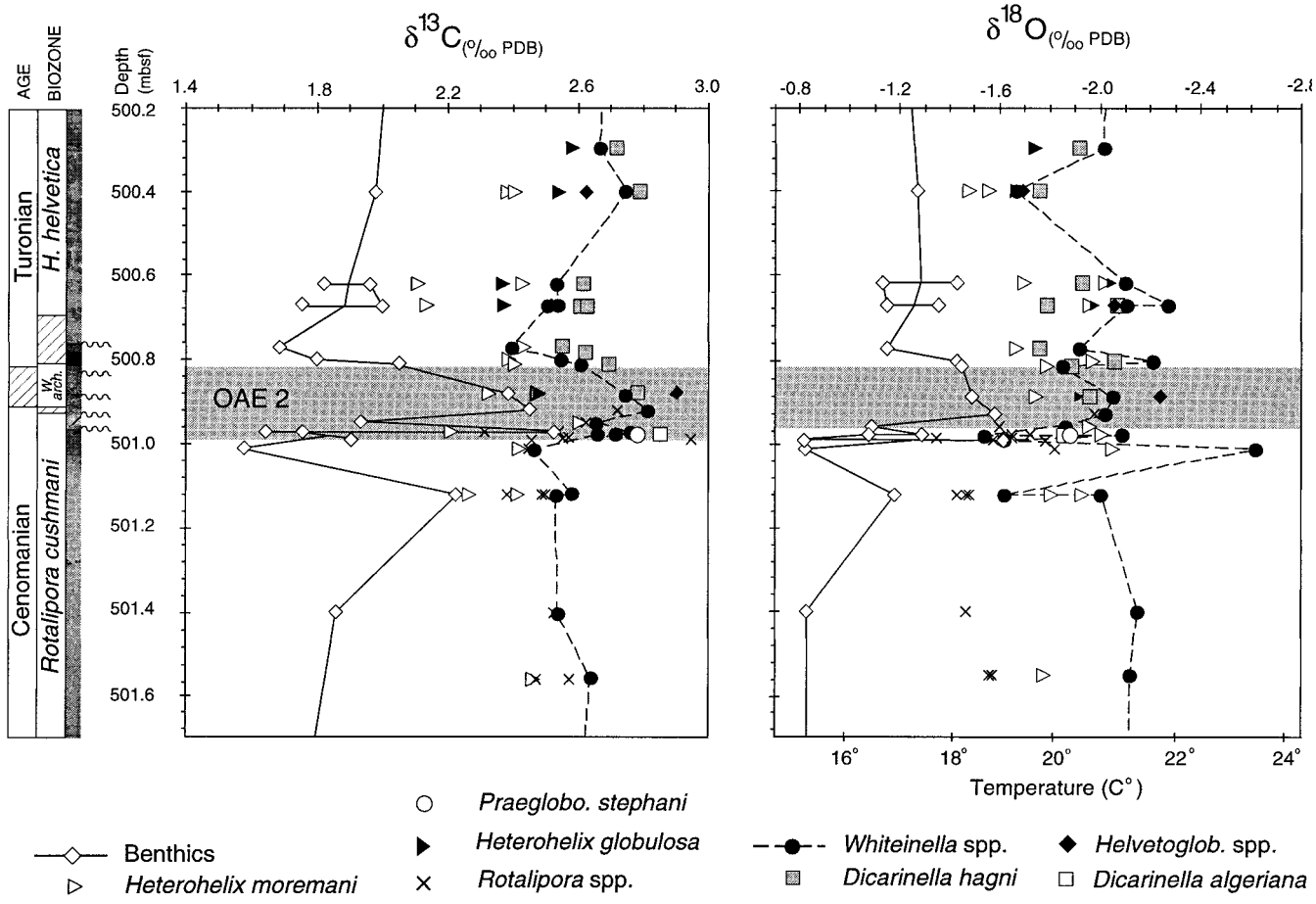

FIGURE 12. Oxygen and carbon isotope data for planktic and benthic foraminifera from Section 1050C-21R-1.

in most Cenomanian and Turonian samples. The smallest $\delta^{18}O$ gradient of 0.44‰ occurs within the sample bearing the LO of rotaliporids.

Replicate Sample Analyses

Intraspecific variability determined from replicate stable isotopic analyses of six planktonic foraminifer samples is surprisingly small considering the time averaging that must have occurred within each sample from this condensed CTBI sequence (Table 3). For carbon isotopic analyses nearly all offsets are less than 0.1‰, and the largest offset is a difference of 0.15‰. Most of the $\delta^{18}O$ offsets between replicate samples are also less then 0.1‰, and the highest offset of 0.34‰ occurs in a replicate of *Whiteinella baltica*.

The only ''replicate'' analysis of benthic foraminifer is a sample from 500.97 mbsf containing *Gavelinella* sp., which yielded an offset of 0.15‰ in $\delta^{13}C$ and 0.22‰ in $\delta^{18}O$. These larger values maybe explained by the inclusion of multiple species in the monogeneric analysis. Analysis of the benthic foraminifer taxa *Cibicides* sp. and *Gavelinella* sp. revealed that the latter taxon is more negative in in $\delta^{13}C$ and $\delta^{18}O$ by 0.24 and 0.21‰, respectively.

DISCUSSION

Stratigraphic Completeness of OAE 2 at Site 1050

Gale and others (1993) and Pratt and Threlkeld (1984) have identified a series of bio- and chemostratigraphic events in the Eastbourne section of the Plenus Marl and the Rock Canyon section of the lower Bridge Creek Limestone that can be used to help determine stratigraphic completeness of OAE 2 events. Their studies revealed that three $\delta^{13}C$ peaks should occur in stratigraphically continuous OAE 2 sequences. The first peak in the Eastbourne section is defined by a 1.8‰ $\delta^{13}C$ enrichment that precedes the LO of the planktic foraminifer *R. cushmani* and the LO of the calcareous nannofossil *A. albianus*. This first $\delta^{13}C$ enrichment marks the base of the OAE 2 event. The second $\delta^{13}C$ enrichment is more broadly defined across several meters of section within the uppermost Cenomanian, while the third peak is more sharply defined and occurs in the lowermost Turonian (Gale and others, 1993; Pratt and Threlkeld, 1984). $\delta^{13}C$ values between the first and last peaks at the Eastbourne and Rock Canyon sections are all enriched relative to over- and underlying samples.

The $\delta^{13}C$ record at Site 1050 shows a single enrichment peak that is defined by multiple data points for both planktic

and benthic foraminifera at the level of the debris flow beds. However, the magnitude of the shift is considerably lower than at the Eastbourne and Rock Canyon sections. Corresponding with the $\delta^{13}C$ shift are (1) the extinction of rotaliporids and *G. bentonensis*; (2) a significant benthic foraminifer $\delta^{18}O$ depletion; (3) a decrease in percent calcium carbonate values; and (4) an increase in benthic foraminifer abundance. On the basis of these changes and their chronostratigraphic correlation we identify the interval from 500.92 to 500.81 mbsf as OAE 2. Absence of multiple $\delta^{13}C$ enrichment peaks, sedimentologic evidence for diastems or extremely slow sedimentation, and the abruptness of biostratigraphic changes in planktic foraminifer and calcareous nannofossil assemblages suggest that the OAE 2 interval at Site 1050 is condensed and incomplete. It is possible that the first and second $\delta^{13}C$ peaks found at the Eastbourne and Rock Canyon sections are juxtaposed at Site 1050, as the sample with the most enriched $\delta^{13}C$ value is still within the *R. cushmani* Zone, while the enriched samples above are within the *W. archaeocretacea* Zone. This interpretation is consistent with the biostratigraphic evidence presented above that the contact between the white and gray debris flow beds (or within the gray debris flow unit) is a diastem that spans ~0.5 m.y. This may also explain why an interval enriched in total organic carbon found in OAE 2 sequences in all complete CTB sections (e.g., Schlanger and others, 1987) is not observed at Site 1050.

Cenomanian/Turonian Boundary Thermal Maximum

The warmest benthic foraminifer $\delta^{18}O$ paleotemperatures of the Site 1050 sequence occur within the OAE 2 interval. Assuming that the foraminiferal calcite formed in isotopic equilibrium with Cretaceous seawater, we estimate that the middle bathyal waters (~2000 m paleodepth) ranged between 18 and 19°C during latest Cenomanian and earliest Turonian time. We do not consider these isotopically light values to be an artifact of diagenesis as planktic foraminiferal $\delta^{18}O$ measurements do not show a negative shift that corresponds with the benthic $\delta^{18}O$ record and diagenesis in pelagic chalk settings with shallow burial depths normally drives $\delta^{18}O$ values in the positive rather than negative direction (Schrag and others, 1995).

The benthic foraminiferal warming event across the CTBI is in agreement with evidence for extreme warmth in the north and south polar regions at this time, including the discovery of champsosaur (crocodile-like reptile) remains in the High Canadian Arctic (Tarduno and others, 1998), paleobotanical evidence for mild winter temperatures in the Alaskan North Slope (Spicer and Parrish, 1987; Herman and Spicer, 1997), and warm oxygen isotope paleotemperature estimates from deep water benthic and surface water planktic foraminifera in the circum-Antarctic region (Huber and others, 1995). This middle Cretaceous ''supergreenhouse'' warming may have resulted from an anomalous increase in global magmatism and an increased flux in volcanic CO_2 into the atmosphere and oceans (Tarduno and others, 1998; Kerr, 1998). However, there is a discrepancy between the radioactive dates of the erupted igneous rocks (~93–86 Ma; see references cited in Tarduno and others, 1998) and the timing of the stable isotopic thermal maximum (~94.0–93.0 Ma). Co-occurrence at Site 1050 of volcaniclastic sediments with benthic foraminifera that yielded the warmest temperatures invites further speculation that there was increased global volcanism at CTBI time. But until the discrepancy between the radioactive dates and dating of the peak warming is resolved, CO_2 forcing cannot be seriously considered as the main cause for the CTBI supergreenhouse.

Several authors have suggested that expansion of the OMZ into the lower surface mixed layer caused the extinction of rotaliporids and other deeper dwelling planktic taxa at the onset of OAE 2 (Wonders, 1979; Hart, 1980; Arthur and others, 1987; Erbacher and Thurow, 1997). Based on the oxygen isotope record at Site 1050, we propose that deep water warming could have triggered planktic extinctions by eliminating the thermocline, thereby removing the environmental signal that was essential for reproduction of the deepest dwelling species. Testing of this hypothesis will require recovery of reliable oxygen isotope profiles across the rotaliporid extinction at other sites that are more stratigraphically complete than Site 1050 to verify that the vertical $\delta^{18}O$ gradient was more reduced at the end of the Cenomanian than at any other time within the stratigraphic range of the rotaliporids.

Subtropical Sea Surface Temperatures

Estimates of mid-Cretaceous sea surface temperatures (SSTs) from oxygen isotope values require assumptions about the seawater $\delta^{18}O$ composition in which the measured planktic foraminifera grew. Depleted benthic foraminiferal $\delta^{18}O$ values from deep sea Cenomanian/Turonian boundary sections (e.g., Huber and others, 1995; this study) indicate that the polar regions were too warm to support glacial ice and, thus, the most appropriate estimate for the $\delta^{18}O$ composition of mid-Cretaceous seawater is a value of $-1.2‰_{SMOW}$ (Shackleton and Kennett, 1975). In the modern ocean latitudinal changes in the balance of evaporation and precipitation (the salinity effect) and $\delta^{18}O$ fractionation during vapor transport cause subtropical surface waters to be from 1.0 to 1.5‰ more enriched in $\delta^{18}O$ than the high latitudes (Broecker, 1989). Assuming that the Hadley cells (which control the balance of evaporation and precipitation) occupied their current subtropical position during the geologic past, Zachos and others (1994) applied a correction using the modern latitudinal $\delta^{18}O$ gradient to estimate SSTs for the Paleogene. This correction was subsequently used by Huber and others (1995) to calculate southern high latitude SSTs for the Cretaceous and is applied to the Site 1050 planktic foraminiferal values to estimate subtropical SSTs. The corrected values from Site 1050 are about 2°C warmer than unadjusted estimates (Fig. 13). If the salinity estimate predicted from the General Circulation Model (GCM) simulation for mid-Cretaceous subtropical surface waters by Barron and others (1995) are used instead of the Zachos and others (1994) correction, as was done by Fassell and Bralower (1999), the Site 1050 SST estimates would be about 3°C warmer than the unadjusted estimates.

Planktic species yielding the lowest $\delta^{18}O$ values mostly range between 23 and 25°C, which is within the range of subtropical SSTs today. Heterohelicids from 509.25 mbsf

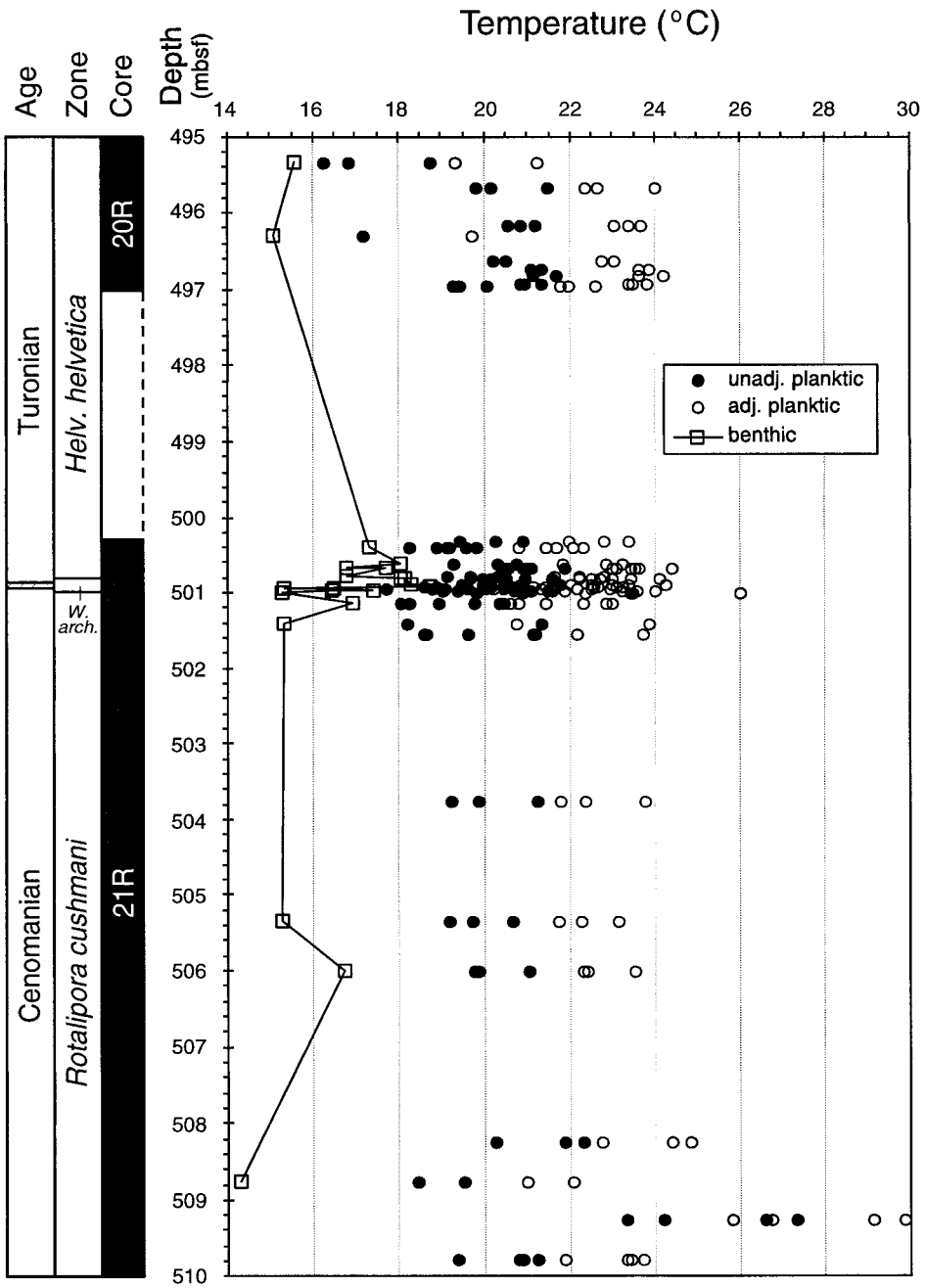

FIGURE 13. Paleotemperature estimates from benthic and planktic foraminiferal $\delta^{18}O$ values across the CTBI of Site 1050. Planktic values are shown as unadjusted and adjusted using the salinity correction of Zachos and others (1994) assuming a modern latitude-salinity relationship during the middle Cretaceous.

yield the warmest SST of the upper Cenomanian-lower Turonian interval (30°C), whereas heterohelicids from 0.5 m higher yield the coolest SST (22°C). Rotaliporids are mostly 3 to 4°C cooler than the co-occurring species yielding the warmest SSTs. The total vertical temperature gradient generally ranges from 6 to 8°C.

The lack of change in the subtropical SSTs suggested by the Site 1050 planktic foraminiferal stable isotopic record contrasts with the dramatic warming suggested from benthic foraminifera from this site and from southern high latitude SSTs (Huber et al., 1995). The cause for this decoupling of surface and deep waters warrants further investigation.

SUMMARY

The Cenomanian/Turonian boundary at Site 1050 is placed at 500.81–500.90 mbsf within a debris flow unit that contains multiple diastems. Correlation of our stable isotopic and biostratigraphic results with CTBI sections in England, Italy and the U.S. Western Interior indicates that al-

though ~0.5 m.y. is missing from the Site 1050 CTBI sequence, part of the OAE 2 interval is nonetheless represented. A 0.8‰ positive shift in benthic foraminifer $\delta^{13}C$ values at the top of the *Rotalipora cushmani* Zone at Site 1050 is correlated with the lowermost $\delta^{13}C$ shift reported in the Eastbourne, Sussex (Gale and others, 1993) and Rock Canyon, Colorado (Pratt and Threlkeld, 1984) sections. Planktic and benthic foraminifera that are enriched in $\delta^{13}C$ immediately above this level are correlated with the lower Turonian portion of OAE 2. The relatively moderate $\delta^{13}C$ enrichment, very low total organic carbon, abundance of benthic foraminifera, and absence of sediment laminations across this interval suggest that the time of peak oxygen minimum zone expansion during OAE 2 is missing at Site 1050.

At the same level as the benthic and planktic foraminifer carbon isotope shifts, the temperature of middle bathyal waters increased from ~15 to ~19°C, which is warmer than any other time during the Cretaceous or Cenozoic. This deep water warming may have caused a breakdown in the vertical structure of the water column, and could explain the extinction of the deeper dwelling planktic foraminiferal taxa, such as *Rotalipora* and *Globigerinelloides bentonensis*. A coeval warming event has been identified from oxygen isotopic records of deep-sea planktic foraminifera in the southern high latitudes and is consistent with paleontological evidence for extreme warmth in the Arctic. On the other hand, sea surface temperature estimates based on planktic foraminiferal $\delta^{18}O$ values from Site 1050 (corrected for the modern day salinity gradient) remain steady throughout the CTBI, varying between 23 to 26°C., which is within the range of subtropical SSTs today.

The mid-Cretaceous ''supergreenhouse'' may have resulted from an increased flux in volcanic CO_2 into the atmosphere and oceans (Tarduno and others, 1998; Kerr, 1998). However, a several million year discrepancy between the radioactive ages of known volcanic episodes and the timing of the thermal maximum needs to be clarified before CO_2 forcing can be accepted as the main cause of the global warming. If increased pCO_2 was the primary mechanism driving the middle Cretaceous supergreenhouse, then climate and ocean models must explain how heat was transported from the tropics to the poles with enough efficiency to maintain a latitudinal thermal gradient profile that was nearly flat.

ACKNOWLEDGMENTS

This study was supported by funds from the Smithsonian Scholarly Studies Program and Walcott Trust to BTH, JOI/USSAC funding for ODP shore-based research to RML, and NSF grant OCE 9819050 to RDN and a post-cruise award from JOI/USSAC for leg 171B. We thank Isabella Premoli Silva and Elisabetta Erba for their constructive reviews; My Le Ducharme for her help with computer graphics; J. Singleton, M. Wapner, and K. Reiter for help editing digital species images; and the Ocean Drilling Program and Bremen Core Repository for making the samples available.

REFERENCES

ARTHUR, M. A., and PREMOLI SILVA, I., 1982, Development of widespread organic carbon-rich strata in the Mediterranean Tethys, *in* Schlanger, S. O., and Cita, M. B. (eds.), Nature of Cretaceous Carbon-Rich Facies, London, Academic Press, p. 7–54.

———, SCHLANGER, S. O., and JENKYNS, H. C., 1987, The Cenomanian-Turonian Oceanic Anoxic Event, II. Paleoceanographic controls on organic-matter production and preservation, *in* Brooks, J. and Fleet, A. J. (eds.), Marine Petroleum Source Rocks, Geological Society Special Publication No. 26, London, p. 401–420.

BARRON, E. J. and WASHINGTON, W. M., 1985, Warm Cretaceous climates: high atmospheric CO2 as a plausible mechanism, *in* Sundquist, E. T. and Broecker, W. S. (eds.), The Carbon Cycle and Atmospheric CO_2: Natural Variations Archaen to Present, American Geophysical Union, Geophysical Monograph no. 32, p. 546–553.

BENSON, W. E., SHERIDAN, R. E. and others, 1978, Initial Reports of the Deep Sea Drilling Project, U.S. Government Printing Office, Washington, DC, v. 44, p. 1–1005.

BOLLI, H. M., 1966, Zonation of Cretaceous to Pliocene marine sediments based on planktonic foraminifera: Boletin Informativo Asociacion Venezolana de Geología, Minería y Petroleo, v. 9, p. 3–32.

BOULTER, M. C., GEE, D., and FISHER, H. C., 1998, Angiosperm radiation at the Cenomanian/Turonian and Cretaceous/Tertiary boundaries: Cretaceous Research, v. 19, p. 107–112.

BRALOWER, T. J., 1988, Calcareous nannofossil biostratigraphy and assemblages of the Cenomanian-Turonian boundary interval: Implications for the origin and timing of oceanic anoxia: Paleoceanography, v. 3, p. 275–316.

———, and BERGEN, J. A., 1998, Cenomanian-Santonian calcareous nannofossil biostratigraphy of a transect of cores drilled across the Western Interior Seaway: *in* Arthur, M. A., and Dean, W. E. (eds.), The Cretaceous Western Interior Drilling Program, Society of Economic Paleontologists and Mineralogists, Concepts in Sedimentology and Paleontology, 6, p. 15–35.

———, FULLAGAR, P. D., PAULL, C. K., DWYER, G. S., and LECKIE, R. M., 1997, Mid-Cretaceous strontium-isotope stratigraphy of deep-sea sections: Geological Society of America Bulletin, v. 109, p. 1421–1442.

———, SLITER, W. V., ARTHUR, M. A., LECKIE, R. M., ALLARD, D., and SCHLANGER, S. O., 1993, Dysoxic/anoxic episodes in the Aptian-Albian (Early Cretaceous), *in* Pringle, M. S., Sager, W. W, Sliter, W. V, and Stein, S. (eds.), The Mesozoic Pacific: Geology, Tectonics, and Volcanism: Washington, D.C., American Geophysical Union, Geophysical Monograph 77, p. 5–37.

———, and THIERSTEIN, H. R., 1984, Low productivity and slow deep-water circulation in mid-Cretaceous oceans: Geology, v. 12, p. 614–618.

BYERLY, G. R., 1991, Igneous activity, *in* Salvador, A., ed., The Gulf of Mexico Basin: Boulder, Colorado, Geological Society of America, The Geology of North America, v. J, p. 91–108.

CARON, M., 1985, Cretaceous planktonic foraminifera, *in* Bolli, H. M., Saunders, J. B., and Perch-Nielsen, K., (eds.), Plankton Stratigraphy, Cambridge University Press, Cambridge, p. 17–86.

———, and HOMEWOOD, P., 1983, Evolution of early planktic foraminifera: Marine Micropaleontology, v. 7, p. 453–462.

CUSHMAN, J. A., 1983, Cretaceous species of Guembelina and related genera: Cushman Laboratory for Foraminiferal Research, Contributions, v. 14, p. 2–28.

ELDER, W. P., 1991, Molluscan paleoecology and sedimentation patterns of the Cenomanian-Turonian extinction interval in the southern Colorado Plateau region, *in* Nations, J. D. and Eaton, J. G., (eds.), Stratigraphy, Depositional Environments, and Sedimentary Tectonics of the Western Margin, Cretaceous Western Interior Seayway, Geological Society of America, Boulder, v. Special Paper 260, p. 113–137.

———, GUSTASON, E. R., and SAGEMAN, B. B., 1994, Correlation of basinal carbonate cycles to nearshore parasequences in the Late Cretaceous Greenhorn seaway, Western Interior, U.S.A.: Geological Society of America Bulletin, v. 106, p. 892–902.

ERBA, E., PREMOLI SILVA, I., and WATKINS, D. K., 1996, Cretaceous calcareous plankton stratigraphy of Sites 872 through 879, *in* Haggerty, J. A., Premoli Silva, I., Rack, F., and McNutt, M. K. (eds.), Proceedings of the Ocean Drilling Program, Scientific Results, Volume 144: College Station, Texas, Ocean Drilling Program, p. 157–169.

ERBACHER, J., JÜRGEN, T., and LITTKE, R., 1996, Evolution patterns of radiolaria and organic matter variations: A new approach to identify sea-level changes in mid Cretaceous pelagic environments: Geology, v. 24, p. 499–502.

———, and THUROW, J., 1997, Influence of oceanic anoxic events on the evolution of mid-Cretaceous radiolaria in the North Atlantic and western Tethys: Marine Micropaleontology, v. 30, p. 139–158.

EREZ, J., and LUZ, B., 1983, Experimental paleotemperature equation for planktonic foraminifera: Geochemica et Cosmochimica Acta, v. 47, p. 1025–1031.

GALE, A. S., JENKYNS, H. C., KENNEDY, W. J., and CORFIELD, R.M., 1993, Chemostratigraphy versus biostratigraphy: Data from around the Cenomanian-Turonian boundary: Journal of the Geological Society, London, v. 150, p. 29–32.

GRADSTEIN, F. M., AGTERBERG, F. P., OGG, J. G., HARDENBOL, J., VAN VEEN, P., THIERRY, J., and HUANG, Z., 1994, A Mesozoic time scale: Journal of Geophysical Research, v. 99, p. 24,051–24,074.

HANCOCK, J. M., KENNEDY, W.J., and COBBAN, W. A., 1993, A correlation of the upper Albian to basal Coniacian sequences of northwest Europe, Texas and the United States Western Interior, *in* Caldwell, W. G. E., and Kauffman, E. G.(eds.), Evolution of the Western Interior Basin: St. John's, Geological Association of Canada Special Paper 39, p. 453–476.

HAQ, B. U., HARDENBOL, J., and VAIL, P. R., 1988, Mesozoic and Cenozoic chronostratigraphy and cycles of sea-level change, *in* Wilgus, C. K., Hastings, B., Ross, C., Posamentier, H., Van Wagoner, J., and Kendall, C., (eds.), Sea-level Changes: An Integrated Approach: Tulsa, Society for Economic Geology (SEPM), Special Publication 42, p. 71–108.

HART, M. B., 1980, A water depth model for the evolution of the planktonic Foraminiferida: Nature, v. 286, p. 252–254.

HAYEK, L.-A. C., and BUZAS, M.A., 1997, Surveying Natural Populations: Columbia University Press, New York, p. 1–563.

HERMAN, A., and SPICER, R. A., 1997, New quantitative palaeoclimate data for the Late Cretaceous Arctic: evidence for a warm ocean: Palaeogeography, Palaeoclimatology, Palaeoecology, v. 128, p. 227–251.

HILBRECHT, H., and DAHMER, D. D., 1994, Sediment dynamics during the Cenomanian-Turonian (Cretaceous) Oceanic Anoxic Event in northwestern Germany: Facies, v. 30, p. 63–84.

HUBER, B. T., HODELL, D. A., and HAMILTON, C. P., 1995, Mid- to Late Cretaceous climate of the southern high latitudes: Stable isotopic evidence for minimal equator-to-pole thermal gradients: Geological Society of America Bulletin, v. 107, p. 1164–1191.

HUT, G., 1987, Consultants group meeting on stable isotope reference samples for geochemical and hydrological investigations: Report to Director General of the Institute of Atomic Energy Agency, Vienna, Austria.

JARVIS, I., CARSON, G. A., COOPER, M. K. E., HART, M. B., LEARY, P. N., TOCHER, B. A., HORNE, D., and ROSENFELD, A., 1988, Microfossil assemblages and the Cenomanian-Turonian (Late Cretaceous) oceanic anoxic event: Cretaceous Research, v. 9, p. 3–103.

JUIGNET, P., and BRETON, G., 1992, Mid-Cretaceous sequence stratigraphy and sedimentary cyclicity in the western Paris Basin: Palaeogeography, Palaeoclimatology, Palaeoecology, v. 91, p. 197–218.

KAIHO, K., and HASEGAWA, T., 1994, End-Cenomanian benthic foraminiferal extinctions and oceanic dysoxic events in the northwestern Pacific Ocean: Palaeogeography, Palaeoclimatology, Palaeoecology, v. 111, p. 29–43.

KAUFFMAN, E. G., 1977, Geological and biological overview: western interior Cretaceous basin: The Mountain Geologist, v. 14, p. 75–100.

———, 1984, Paleobiogeography and evolutionary response dynamic in the Cretaceous Western Interior Seaway of North America, *in* Westermann, G. E. G. (ed.), Jurassic-Cretaceous Biochronology and Paleogeography of North America: St. John's, Geological Association of Canada Special Paper 27, p. 273–306.

———, PRATT, L. M. and others, 1985, A field guide to the stratigraphy, geochemistry, and depositional environments of the Kiowa-Skull Creek, Greenhorn, and Niobrara marine cycles in the Pueblo-Canon City area, Colorado, *in* Pratt, L. M., Kauffman, E. G., and Zelt, F. B. (eds.), Fine-grained Deposits and Biofacies of the Cretaceous Western Interior Seaway: Evidence of Cyclic Sedimentatary Processes, Field Trip Guidebook No. 4, Society of Economic Paleontologists and Mineralogists, Tulsa, p. 1–26.

———, SAGEMAN, B. B., KIKRLAND, J. I., ELDER, W. P., HARRIES, P. J., and VILLAMIL, T., 1993, Molluscan biostratigraphy of the Cretaceous western interior basin, North America, *in* Caldwell, W. G. E., and Kauffman, E. G. (eds.), Evolution of the Western Interior Basin: St. John's, Geological Association of Canada Special Paper 39, p. 397–434.

KERR, A. C., 1998, Oceanic plateau formation: a cause of mass extinction and black shale deposition around the Cenomanian-Turonian boundary?: Journal of the Geological Society of London, v. 155, p. 619–626.

KIRKLAND, J. I., 1991, Lithostratigraphic and biostratigraphic framework for the Mancos Shale (late Cenomanian to middle Turonian) at Black Mesa, northeastern Arizona, *in* Nations, J. D., and Eaton, J. G. (eds.), Stratigraphy, Depositional Environments, and Sedimentary Tectonics of the Western Margin, Cretaceous Western Interior Seaway: Boulder, Geological Society of America Special Paper 260, p. 85–111.

KILLINGLEY, J. S., 1983, Effects of diagenetic recrystallization on 180/160 values of deep-sea sediments: Nature, v. 301, p. 594–597.

LECKIE, R. M., 1985, Foraminifera of the Cenomanian-Turonian boundary interval, Greenhorn Formations, Rock Canyon Anticline, Pueblo Colorado, *in* Pratt, L, Kauffman, E. G., and Zelt, F. B., (eds.), Fine-grained Deposits and Biofacies of the Cretaceous Western Interior Seaway: Evidence of Cyclic Sedimentary Processes, Field Trip Guidebook No. 4, Society of Economic Paleontologists and Mineralogists, Tulsa, p. 139–149.

———, 1989, A paleoceanographic model for the early evolutionary history of planktonic foraminifera: Palaeogeography, Palaeoclimatology, Palaeoecology, v. 73, p. 107–138.

———, YURETICH, R. F., WEST, O. L. O., FINKELSTEIN, D., and SCHMIDT, M., 1998, Paleoceanography of the southwestern Western Interior Sea during the time of the Cenomanian-Turonian boundary (Late Cretaceous), *in* Dean, W., and Arthur, M. A. (eds.), Stratigraphy and Paleoenvironments of the Cretaceous Western Interior Seaway, USA, SEPM Concepts in Sedimentology and Paleontology No. 6, SEPM (Society for Sedimentary Geology), Tulsa, OK, p. 101–126.

LEITHOLD, E. L., 1994, Stratigraphical architecture at the muddy margin of the Cretaceous Western Interior Seaway, southern Utah, Sedimentology, v. 41, p. 521–542.

MONECHI, S., and THIERSTEIN, H. R., 1985, Late Cretaceous-Eocene nannofossil and magnetostratigraphic correlations near Gubbio, Italy: Marine Micropaleontology, v. 9, p. 419–440.

NEDERBRAGT, A. J., 1991, Late Cretaceous biostratigraphy and development of Heterohelicidae (planktic foraminifera): Micropaleontology, v. 37, p. 329–372.

———, ERLICH, R. N., FOUKE, B. W., and GANSSEN, G. M., 1998, Palaeoecology of the biserial planktonic foraminifer *Heterohelix moremani* (Cushman) in the late Albian to middle Turonian circum-North Atlantic: Palaeogeography, Palaeoclimatology, Palaeoecology, v. 144, p. 115–133.

NORRIS, R. D., KROON, D., and KLAUS, A., 1998, Proceedings of the Ocean Drilling Program, Initial Reports, Ocean Drilling Program, College Station, TX, v. 171B, p. 1–749.

PAUL, C. R. C., MITCHELL, S., LAMOLDA, M., and GOROSTIDI, A., 1994, The Cenomanian-Turonian boundary event in northern Spain: Geological Magazine, v. 131, p. 801–817.

PRATT, L. M., ARTHUR, M. A., DEAN, W. E., and SCHOLLE, P. A., 1993, Paleo-oceanographic cycles and events during the Late Cretaceous in the Western Interior Seaway of North America, *in* Caldwell, W. G. E., and Kauffman, E. G. (eds.), Evolution of the Western Interior Basin: St. John's, Geological Association of Canada Special Paper 39, p. 333–353.

———, and THRELKELD, C. N., 1984, Stratigraphic significance of 12C/!2C ratios in mid-Cretaceous rocks of the Western Interior, U.S.A., *in* Stott, D. F. and Glass, D. J. (eds.), The Mesozoic of Middle North America, Memoir of the Canadian Society of Petroleum Geologists, v. 9, p. 305–312.

PREMOLI SILVA, I., ERBA E., SALVINI G., LOCATELLI C., VERGA D.,

1999, Biotic changes in Cretaceous oceanic anoxic events of the Tethys: Journal of Foraminiferal Research, v. 29, p. in press.

———, and SLITER, W. V., 1994, Cretaceous planktonic foraminiferal biostratigraphy and evolutionary trends from the Bottaccione Section, Gubbio, Italy: Palaeontographica Italia, v. 81, p. 2–90.

ROBASZYNSKI, F., CARON, M. (coordinators) and European Working Group on Planktonic Foraminifera, 1979, Atlas of Mid Cretaceous Planktonic Foraminifera (Boreal Sea and Tethys), Cahiers de Micropaléontologie, 1 and 2, C.N.R.S., Paris, 185 pp. & 181 pp.

———, ———, DUPUIS, C., AMEDRO, F., GONZALEZ DONOSO, J.-M., LINARES, D., HARDENBOL, J., GARTNER, S., CALANDRA, F., and DELOFFRE, R., 1990, A tentative integrated stratigraphy in the Turonian of central Tunisia: Formations, zones, and sequential stratigraphy in the Kalaat Senan area: Bull. Centres Rech. Explor.-Prod. Elf-Aquitaine, v. 14, p. 213–384.

———, HARDENBOL, J., CARON, M., AMEDRO, F., DUPUIS, C., GONZALEZ DONOSO, J.-M., LINARES, D., GARTNER, S., 1993, Sequence stratigraphy in a distal environment: the Cenomanian of the Kalaat Senan region (central Tunisia): Bull Centres Rech. Explor.-Prod. Elf-Aquitaine, v. 17, p. 395–433.

SAGEMAN, B. B., RICH, J., ARTHUR, M. A., BIRCHFIELD, G. E., and DEAN, W. E., 1997, Evidence for Milankovitch periodicities in Cenomanian-Turonian lithologic and geochemical cycles, western interior U.S.A.: Journal of Sedimentary Research, v. 67, p. 286–302.

SAHAGIAN, D., PINOUS, O., OLFERIEV, A., and ZAKHAROV, V., 1996, Eustatic curve for the Middle Jurassic-Cretaceous based on Russion Platform and Siberian stratigraphy: zonal resolution: American Association of Petroleum Geologists Bulletin, v. 80, p. 1433–1458.

SCHLANGER, S. O., ARTHUR, M. A., JENKYNS, H. C., and SCHOLLE, P. A., 1987, The Cenomanian-Turonian Oceanic Anoxic Event, I. Stratigraphy and distribution of organic carbon-rich beds and the marine $\delta^{13}C$ excursion, *in* Brooks, J. and Fleet, A. J. (eds.), Marine Petroleum Source Rocks, Geological Society Publication No. 26, p. 371–399.

———, and JENKYNS, H. C., 1976, Cretaceous Oceanic Anoxic Events: Causes and consequences: Geologie en Mijnbouw, v. 55, p. 179–184.

SCHOLLE, P. A., and ARTHUR, M. A., 1980, Carbon isotope fluctuations in Cretaceous pelagic limestones: potential stratigraphic and petroleum exploration tool: American Association of Petroleum Geologists Bulletin, v. 64, p. 67–87.

SCHRAG, D. P., DEPAOLO, D. J., and RICHTER, F. M., 1995, Reconstructing past sea surface temperatures: correcting for diagenesis of bulk marine carbonate: Geochimica et Cosmochimica Acta, v. 59, p. 2265–2278.

SHACKLETON, N. J., and KENNETT, J. P., 1975, Paleotemperature history of the Cenozoic and the initiation of Antarctic glaciation: oxygen and carbon isotope analysis in DSDP sites 277, 279, and 280, *in* Kennett, J. P., Houtz, R. E. and othersand others, Initial Reports of the Deep Sea Drilling Project, U.S. Government Printing Office, Washington, v. 29, p. 743–755.

SHANNON, C. E., 1948, A mathematical theory of communication: Bell System Technical Journal, v. 27, p. 379–423, 623–656.

SIGURDSSON, H., LECKIE, R. M., ACTON, G., and others, 1997, Proceedings of the Ocean Drilling Program, Initial Reports, v. 165: College Station, Texas, Ocean Drilling Program, 862 p.

SISSINGH, W., 1977, Biostratigraphy of Cretaceous calcareous nannoplankton: Geologie en Mijnbouw, v. 56, p. 37–50.

SPICER, R. A., and PARRISH, J. T., 1987, Plant megafossils, vertebrate remains and paleoclimate of the Kogosukruk Tongue (Late Cretaceous), North Slope, Alaska: United States Geological Survey Circular, v. 998, p. 47–48.

SPOONER, H. V., JR., 1964, Basal Tuscaloosa sediments, east-central Louisiana: American Association of Petroleum Geologists Bulletin, v. 48, p. 1–21.

TARDUNO, J., BRINKMAN, D. B., RENNE, P. R., COTTRELL, R. D., SCHER, H., and CASTILLO, P., 1998, Evidence for extreme climatic warmth from Late Cretaceous Arctic vertebrates: Science, v. 282, p. 2241–2244.

THUROW, J., BRUMSACK, H.-J., RULLKOTTER, J., LITTKE, R., and MEYERS, P., 1992a, The Cenomanian/Turonian boundary event in the Indian Ocean—a key to understand the global picture, *in*: Synthesis of Results from Scientific Drilling in the Indian Ocean: American Geophysical Union, Geophysical Monograph 70, p. 253–273.

———, ERBACHER, J., and STRAUSS, H., 1992b, Radiolarian mass abundance/high diversity, stable isotope variations, black shale sedimentations and sea level changes in the mid-Cretaceous—an integrated approach: Geomar Report, v. 15, p. 281–282.

WEST, O. L. O., LECKIE, R. M., and SCHMIDT, M., 1998, Foraminiferal paleoecology and paleoceanography of the Greenhorn Cycle along the southwestern margin of the U.S. Western Interior Seaway, *in* Dean, W., and Arthur, M. A. (eds.), Stratigraphy and Paleoenvironments of the Western Interior Seaway, USA, SEPM Concepts in Sedimentology and Paleontology No. 6: Society for Sedimentary Geology (SEPM), Tulsa, OK, 79–99.

ZACHOS, J. C., STOTT, L. D., and LOHMANN, K. C., 1994, Evolution of early Cenozoic marine temperatures: Paleoceanography, v. 9, p. 353–387.

Received 23 April 1999
Accepted 13 July 1999

SPECIES LIST

Dicarinella algeriana (Caron) 1966 (Plate 3, Figs. 1–2): This taxon closely resembles *Praeglobotruncana stephani* but is distinguished by the presence of two keels on all but the last chamber. *Dicarinella algeriana* is morphologically similiar to *Praeglobotruncana imbricata* but is distinguished from the latter taxon by its lobate periphery and weaker calcification of its spiral sutures. Both taxa have a moderate trochospire with a distinctly biconvex edge view. The illustrated specimen has a more pinched peripheral margin than most specimens included in this species.

Dicarinella canaliculata (Reuss) 1854 (Plate 3, Figs. 5, 9–10)

Dicarinella sp. aff. *D. canaliculata* (Reuss) (Plate 2, Figs. 18–19)

Dicarinella hagni (Scheibnerova) 1962 (Plate 3, Figs. 11–12): *Dicarinella hagni* is characterized by its closely-spaced keels, low trochospire, and inflated chambers on the umbilical side giving the test a distinctively asymmetrical edge view.

Dicarinella imbricata (Mornod) 1950 (Plate 3, Figs. 6–8): *Dicarinella imbricata* is morphologically similar to *D. algeriana* but is distinguished by its distinctly compact test, better developed peripheral keels, and well-developed beaded sutures on the spiral side.

Globigerinelloides bentonensis (Morrow) 1934 (Plate 1, Figs. 5, 9)

Globigerinelloides sp.: This is a small form with 7–8 chambers that increase more gradually in size in the final whorl than *G. bentonensis*.

Hedbergella delrioensis (Carsey) 1926 (Plate 1, Figs. 6–8)

Hedbergella hoelzli (Hagn and Zeil) 1954: This taxon is the most compressed of all the trochospirally coiled taxa encountered in this study, and it is also distinctly more coarsely pustulose than the other trochospiral taxa.

Hedbergella planispira (Tappan) 1940 (Plate 1, Figs. 10–12)

Hedbergella cf. *H. simplicissima* (Magné and Sigal) 1954 (Plate 1, Figs. 13, 17, 18): The specimens differ from *H. simplicissima* s.s. in being somewhat compressed like *Whiteinella archeocretacea*, but they lack the umbilical-extraumbilical aperture of the latter taxon. The axial compression and apertural characteristics of the Site 1050C specimens resemble *H. flandrini* but the chambers lack the distinctive elongation of this taxon.

Helvetoglobotrunca helvetica (Bolli) 1945 (Plate 2, Figs. 3–5, 9–10, 14): This species is differentiated from *H. praehelvetica* based on flattening of the dorsal chamber surfaces and presence of a keel on the peripheral margin of all chambers in the final whorl.

Helvetoglobotrunca praehelvetica (Trujillo) 1960 (Plate 2, Figs. 15–17)

Heterohelix globulosa (Ehrenberg) 1840 (Plate 1, Figs. 1–2): Examination of the holotype and paratypes of *Heterohelix reussi* (Cushman, 1938) reveals a wide range of morphologic variation and no significant difference from our concept of *H. globulosa*. Thus, we treat the latter species as the senior synonym of the former. The *H. globulosa* from Site 1050 all have a relatively large proloculus, as shown by the illustrated specimen.

Heterohelix moremani (Cushman) 1938 (Plate 1, Figs. 3–4)

Marginotruncana renzi (Gandolfi) 1942 (Plate 3, Figs. 13–15)

Marginotruncana schneegansi (Sigal) 1952

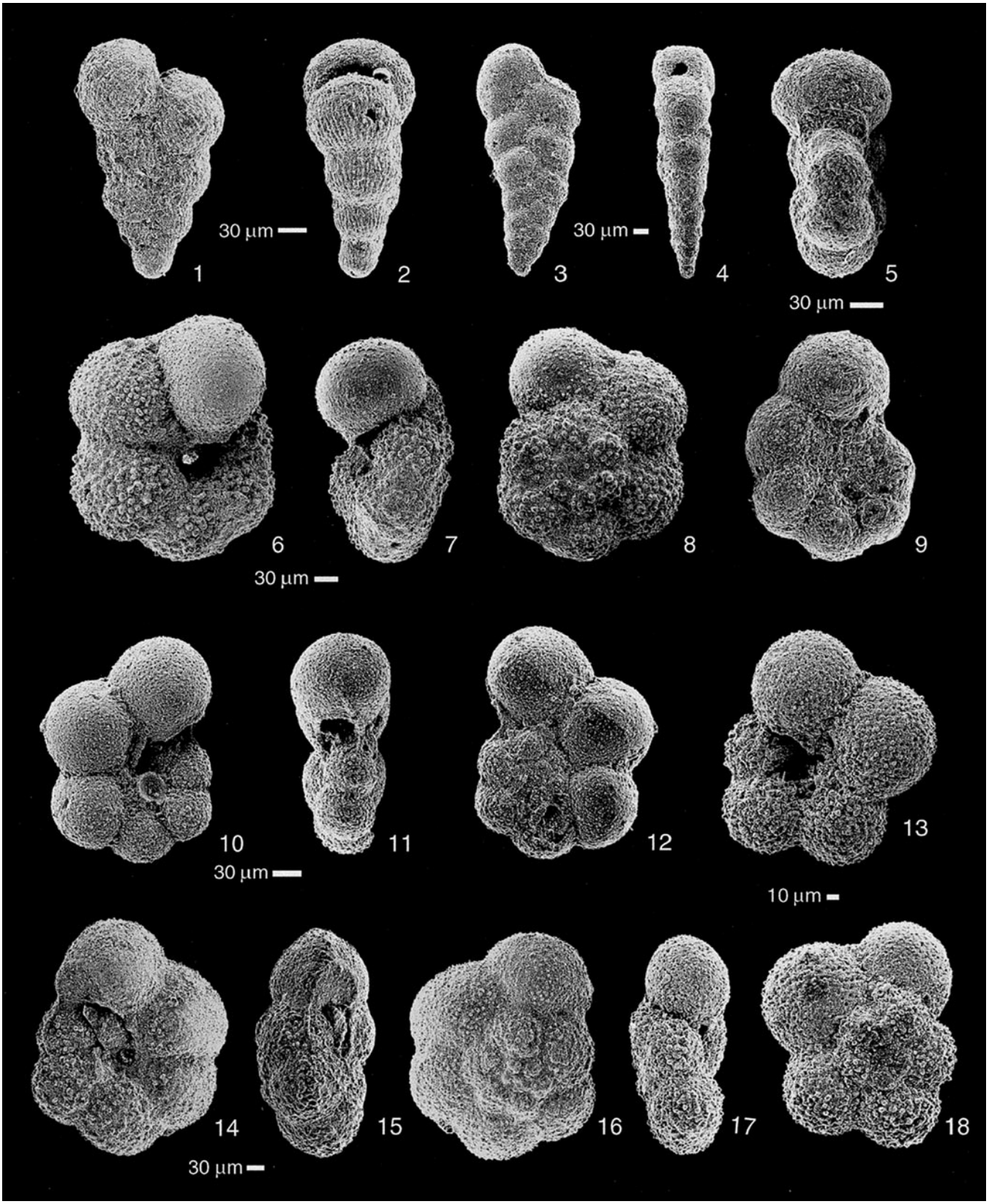

PLATE 1

1–2 Side and edge views of *Heterohelix globulosa* (Ehrenberg), Sample 1050C-20R-5, 37–38 cm. **3–4** Side and edge views of *Heterohelix moremani* (Cushman), Sample 1050C-23R-1, 4–5 cm. **5, 9** Umbilical and edge views of *Globigerinelloides bentonensis* (Morrow), Sample 1050C-21R-1, 81–82 cm. **6–8** Umbilical, edge, and spiral views of *Hedbergella delrioensis* (Carsey), Sample 1050C-26R-2, 56–57 cm. **10–12** Umbilical, edge, and spiral views of *Hedbergella planispira* (Tappan), Sample 1050C-20R-3, 38–41 cm. **13, 17, 18** Umbilical edge, and spiral views of *Hedbergella simplicissima* (Magné and Sigal), Sample 1050C-20R-3, 38–41 cm. **14–16** Umbilical, edge, and spiral views of *Praeglobotruncana aumalensis* (Sigal), Sample 1050C-21R-1, 68–69 cm. Scale bar shown for each specimen.

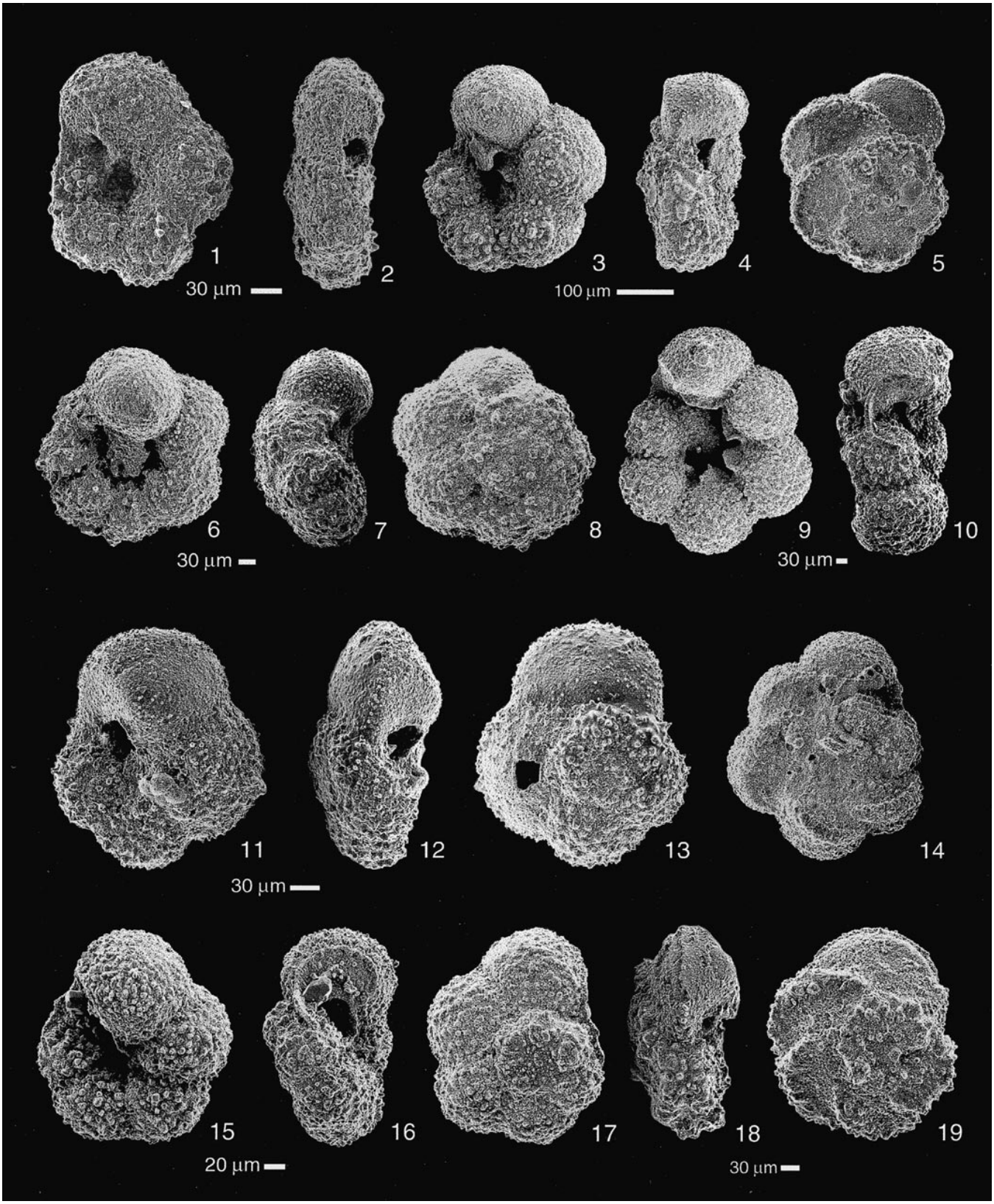

PLATE 2

1, 2 Umbilical and edge views of *Whiteinella archaeocretacea* Pessagno, Sample 1050C-21R-1, 72–73 cm. **3–5** Umbilical, edge and spiral views of *Helvetoglobotrunca helvetica* (Bolli), Sample 1050C-20R-3, 38–41 cm. **6–8** Umbilical, edge and spiral views of *Whiteinella brittonensis* (Loeblich & Tappan), Sample 1050C-21R-1, 61–62 cm. **9–10, 14** Umbilical, edge and spiral views of *Helvetoglobotrunca helvetica* (Bolli), Sample 1050C-20R-3, 129–132 cm. **11–13** Umbilical, edge and spiral views of *Whiteinella inornata* (Bolli), Sample 1050C-21R-1, 76.5–77.5 cm. **15–17** Umbilical, edge, and spiral views of *Helvetoglobotrunca praehelvetica* (Trujillo), Sample 1050C-20R-3, 38–41 cm. **18–19** Umbilical, edge views of *Dicarinella* sp. aff. *D. canaliculata* (Reuss), Sample 1050C-21R-1, 0–1 cm. Scale bar shown for each specimen.

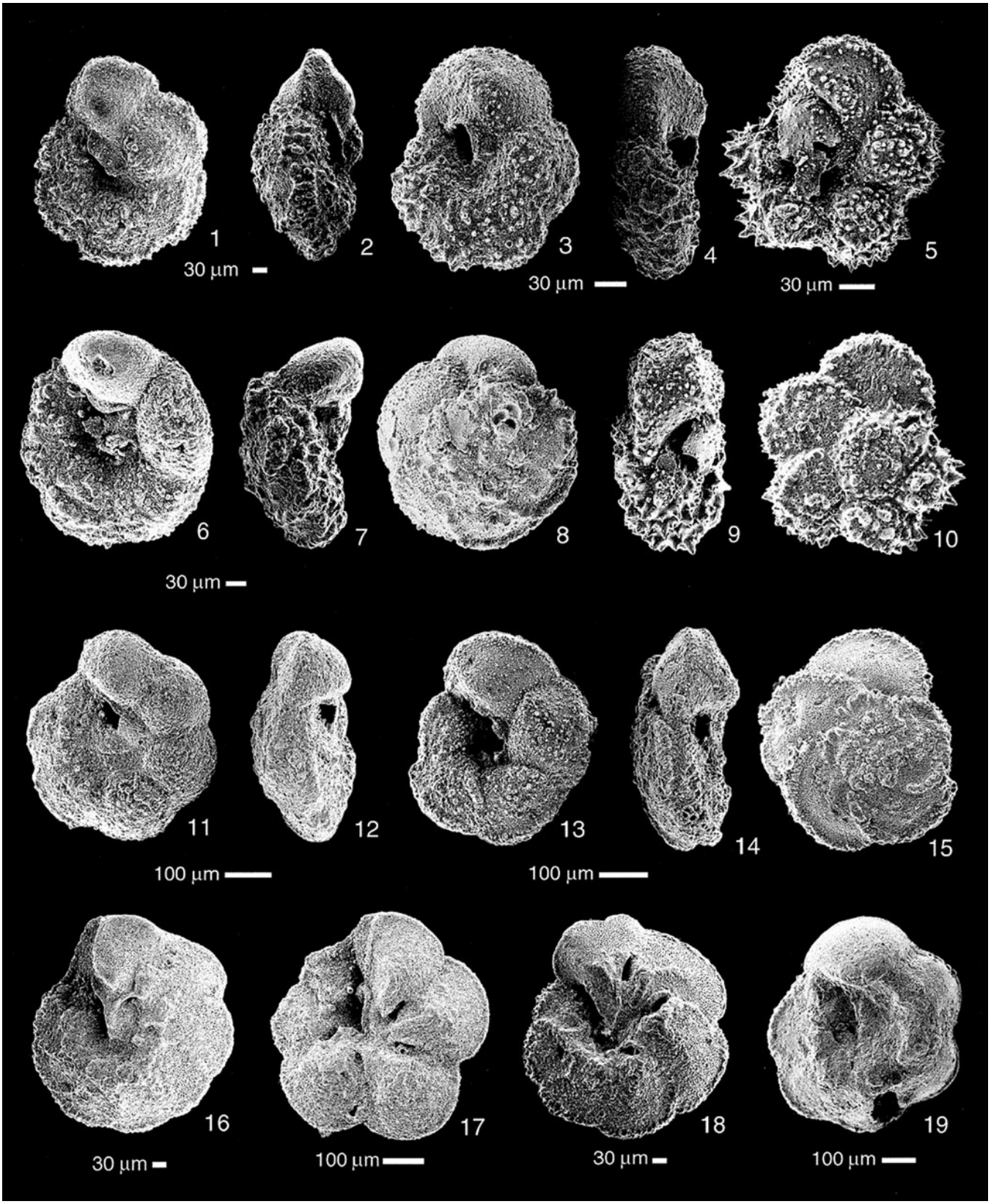

PLATE 3

1–2 Umbilical and edge views of *Dicarinella algeriana* (Caron), Sample 1050C-21R-1, 76.5–77.5 cm. **3, 4** Umbilical and edge views of *Praeglobotruncana* cf. *P. delrioensis* (Plummer), Sample 1050C-21R-1, 76.5–77.5 cm. **5, 9, 10** Umbilical, edge, and spiral views of *Dicarinella canaliculata* (Reuss), Sample 1050C-21R-1, 0–1 cm. **6–8** Umbilical, edge, and spiral views of *Dicarinella imbricata* (Mornod), Sample 1050C-21R-1, 68–69 cm. **11–12** Umbilical and edge views of *Dicarinella hagni* (Scheibnerova), Sample 1050C-21R-1, 72–73 cm. **13–15** Umbilical, edge, and spiral views of *Marginotruncana renzi* (Gandolfi), Sample 1050C-21R-1, 0–1 cm. **16** Umbilical view of *Rotalipora greenhornensis* (Morrow), Sample 1050C-21R-7, 105–108 cm. **17** Umbilical view of *Rotalipora cushmani* (Morrow), Sample 1050C-21R-3, 56–59 cm. **18** Umbilical view of *Rotalipora* aff. *R. greenhornensis* (Morrow), Sample 1050C-25R-3, 60–62 cm. **19** Umbilical view of *Rotalipora deekei* (Franke), Sample 1050C-21R-1, 75–76 cm. Scale bar shown for each specimen.

Marginotruncana? sp.: These small forms are assigned to *Marginotruncana* based on the presence of faint, horseshoe-shaped, raised umbilical sutures, but preservation is too poor for more definite identification.
Praeglobotruncana aumalensis (Sigal) 1952 (Plate 1, Figs. 14–16)
Praeglobotruncana cf. *P. delrioensis* (Plummer) 1931 (Plate 3, Figs. 3–4): Forms included in this taxon are not as lobate as *P. delrioensis* and have a poorly developed keel band. These may be juvenile forms of *Dicarinella*.
Praeglobotruncana gibba Klaus 1960
Praeglobotruncana stephani (Gandolfi) 1942
Rotalipora cushmani (Morrow) 1934 (Plate 3, Fig. 17)
Rotalipora deekei (Franke) 1925 (Plate 3, Fig. 19)
Rotalipora greenhornensis (Morrow) 1934 (Plate 3, Fig. 16)
Rotalipora aff. *R. greenhornensis* (Morrow) 1938 (Plate 3, Fig. 18): This morphotype consistently has fewer chambers and a more lobate peripheral outline than typical *R. greenhornensis*.
Rotalipora sp.
Whiteinella aprica (Loeblich & Tappan) 1961
Whiteinella archaeocretacea Pessagno, 1967 (Plate 2, Figs. 1–2)
Whiteinella baltica Douglas & Rankin, 1969
Whiteinella brittonensis (Loeblich & Tappan) 1961 (Plate 2, Figs. 6–8)
Whiteinella inornata (Bolli) 1957 (Plate 2, Figs. 11–13)